

Bloch Oscillations of Cold Atoms in a Cavity: Effects of Quantum Noise

B. Prasanna Venkatesh¹ and D. H. J. O'Dell¹

¹*Department of Physics and Astronomy, McMaster University,
1280 Main St. W., Hamilton, ON, L8S 4M1, Canada*

We extend our theory of Bloch oscillations of cold atoms inside an optical cavity [Venkatesh *et al.*, Phys. Rev. A **80**, 063834 (2009)] to include the effects of quantum noise. The noise acts as a form of quantum measurement backaction by perturbing the coupled dynamics of the atoms and the light. We take it into account by solving the Heisenberg-Langevin equations for linearized fluctuations about the atomic and optical meanfields and examine how this influences the signal-to-noise ratio of a measurement of external forces using this system. In particular, we investigate the effects of changing the number of atoms, the intracavity lattice depth, and the atom-light coupling strength, and show how resonances between the Bloch oscillation dynamics and the quasiparticle spectrum have a strong influence on the signal-to-noise ratio. One of the hurdles we overcome along the way is the proper treatment of fluctuations about *time-dependent* meanfields in the cold atom cavity-QED context.

PACS numbers: 37.30.+i, 42.50.Lc, 37.10.Vz, 37.10.Jk, 06.20.-f

I. INTRODUCTION

When quantum particles in a periodic potential of period d are subject to a weak additional constant force F they do not uniformly accelerate like free particles, but instead undergo Bloch oscillations [1] at an angular frequency given by:

$$\omega_B = Fd/\hbar. \quad (1)$$

Bloch oscillations (BOs) of cold atoms in optical lattices were first observed in 1996 by uniformly accelerating the lattice [2]: in a frame co-moving with the lattice the atoms experience a constant force. At about the same time, the accelerating lattice method was used to observe Wannier-Stark ladders [3], which are a different aspect of the same “tilted lattice” physics. The method has subsequently been employed to realize beam splitters for atom optics capable of large momentum transfers, see, e.g. [4].

In gravity-driven BOs the lattice is held fixed in space but oriented vertically so that gravity provides the force $F_g = mg$ on atoms of mass m . From Eq. (1), a measurement of ω_B corresponds to a measurement of the applied force F if we know d/\hbar . This Bloch oscillator may be viewed as an interferometer in momentum space [5] and has been experimentally demonstrated by a number of groups [6–9]. For example, the experiment [9] used gravity-driven BOs of strontium atoms to measure the local acceleration due to gravity at the level of $\Delta g/g = 5 \times 10^{-6}$. Like any interferometer, long coherence times are crucial for precision measurements and in [9] the BOs were coherent over 7 s, corresponding to ≈ 4000 oscillations. This remarkable degree of coherence was greatly facilitated by the choice of strontium atoms, which have very weak s -wave scattering, and thus dynamical instabilities normally associated with superflow in lattices [10, 11] were highly suppressed. Variations on this scheme that improve the visibility of the BOs, including frequency [12] and amplitude [13, 14] modulation of the lattice, have allowed for the measurement of gravity

at the level of $\Delta g/g = 10^{-9}$. In these latest experiments the BOs were coherent for over 20 seconds.

The experiments referred to above all involve destructive measurements of the BOs due to the nature of the imaging process of the atoms, whether it be *in situ* or by a time-of-flight technique after the lattice has been switched off [14]. Therefore, a precision measurement of ω_B by the above methods requires that the experiment be re-run many times, each run being for a slightly different hold time, so that the oscillations can be accurately mapped out. This not only takes a long time, but also requires that the initial conditions be recreated as faithfully as possible for each run.

In [15] we proposed a scheme for continuous (i.e. non-destructive) measurements of BOs based upon placing the atoms inside a Fabry-Perot optical resonator which would allow for an estimate of ω_B from the data acquired over a single run. A related scheme has also been independently proposed for ring cavities [16]. The periodic potential is now provided by the standing wave of light which forms inside the cavity when it is pumped by a laser. Orienting the cavity vertically, the atoms execute BOs along the cavity axis as depicted in Fig. 1. The enhanced atom-light coupling inside a high-Q cavity means that the oscillating atoms imprint a detectable periodic modulation on both the phase and amplitude of the light which can be seen either in transmission or reflection. Thus, the measurement is performed upon the light leaking out of the cavity rather than directly upon the atoms.

The strong atom-light coupling that can be realized in cavity-QED stands in contrast to the case of optical lattices in free space where the atoms exert only a tiny backaction upon the light. The optical dipole interaction between a single cavity photon and a single atom is characterized by the Rabi frequency $g_0 = (\mu/\hbar)\sqrt{\hbar\omega_c/(\epsilon_0 V)}$, where ω_c and V are the frequency and volume of the relevant cavity mode and μ is the atomic transition dipole moment. Defining the cooperativity $C \equiv g_0^2/(2\gamma\kappa)$, where 2γ is the spontaneous emission rate of the atom

in free space and 2κ is the energy damping rate of the cavity, $1/C$ is the number of atoms required to strongly perturb the light field. The normal mode splitting that results from strong coupling has been directly observed in a number of cold atom optical cavity experiments [17–20]. In the experiment [20], which was performed with a Bose-Einstein condensate, the cooperativity was $C = 145$. Even more pertinently, these systems have been used to detect the presence of single atoms [21–23], as well as to follow their dynamics in real time [24, 25]. The collective dynamics of ultracold atomic gases have also been tracked using cavities [26–28]. The key experimental steps necessary for the continuous monitoring of BOs in a cavity have, therefore, already been demonstrated.

The rub with any continuous measurement scheme is measurement backaction. In cavities this backaction typically takes the form of cavity photon number fluctuations which lead to random force fluctuations on the atoms, as is evident in the erratic nature of the single atom trajectories seen in the experiments [24, 25] referred to above. In the many atom context, quantum measurement backaction generally manifests itself in a heating of the atom cloud (although under some circumstances it can lead to cooling [29]). In the cavity-optomechanical regime (where the collective motion can be modelled as a harmonic oscillator of angular frequency ω) the heating rate is expected to be $R = (x_{\text{zpf}}/\hbar)^2 S_{\mathcal{FF}}(-\omega)$ [30], where x_{zpf} is the zero-point fluctuation and $S_{\mathcal{FF}}$ is the spectral density of the force fluctuations (which is directly proportional to the cavity photon number fluctuations). This heating rate is in agreement with observations when convolved with technical fluctuations [31].

In the system considered in this paper (see Fig. 1), we can divide the backaction into two types. One type comes from the fact that the atoms sit in an optical lattice whose depth is periodically modulated in time at the frequency ω_B due to the effect of BOs. This backaction is a classical effect in the sense that it occurs even when the light field is treated classically (no photons). The nonlinearity that arises from this backaction can lead to swallowtail loops in the atomic band structure [32, 34] that mimics the effects of direct atom-atom interactions [35–38]. These loops are the counterpart in the atomic wave function of optical bistability in the light [26–28, 33]. The second type of backaction arises only when the fluctuations due to the discrete photon nature of the light field are taken into account and is related to the heating effect mentioned above. The characteristic frequency of these latter fluctuations is κ which is much larger than ω_B .

The first type of backaction was analyzed in our previous paper [15] where our main aim was to show that, despite the self-generated time modulation of the intracavity optical lattice, the Bloch acceleration theorem still applies and the BO frequency is not modified (although harmonics can be generated). This latter result is clearly very important if the cavity BO method is to be used for precision measurements and may be viewed as a conse-

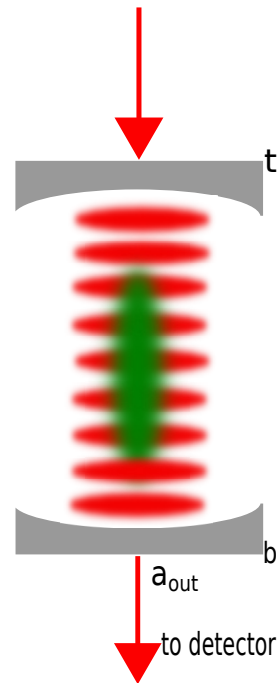


FIG. 1. (Color online) Schematic of the precision measurement proposal in [15]. A dilute cloud of cold atoms undergoes BOs in the combined intracavity lattice potential and the acceleration due to gravity. The transmitted light field's intensity and phase are modulated at the Bloch frequency. A in-situ precise measurement of the Bloch frequency (and hence the force) can be performed by detecting the transmitted light.

quence of the fact that the formula (1) does not depend on the depth of the lattice, only its spatial period. An estimate of the effects of the second type of backaction was also given in our previous paper, but this estimate was obtained under the assumption that the photon number fluctuations were purely due to the photon shot noise found in a coherent state of light. This ignores the correlations that build up between the atoms and the light inside the cavity and our main aim in this paper is to solve the dynamics of the coupled photon and atom fluctuations systematically from first principles and thereby capture these correlations. This will allow us to properly determine the sensitivity of the measurement of the Bloch frequency to quantum fluctuations.

The plan of this paper is as follows: in Section II we introduce the physical system, the associated hamiltonian, and the equations of motion. We then review in Sections III and IV the meanfield approximation and the associated numerical results which were the focus of our previous paper [15], before introducing in Section V the main model to be treated in this paper which adds quantum fluctuations. This is an elaboration of the linearization approach presented in, e.g. [39–41], to include a time-dependent meanfield component (due to the BOs). The fluctuations correspond to quasiparticles (excitations out of the meanfield), and their spectrum is analyzed in Sec-

tion VI and then used to help interpret the numerical results for the quantum dynamics presented in Section VII. We also develop a simple rate equation picture, valid in the weak coupling regime, to help us understand the rate of quasiparticle excitation. Following this we change gears slightly and apply the above results to investigate how quantum fluctuations affect a precision measurement of ω_B by calculating the signal-to-noise ratio (SNR). We present the theory of lying behind these calculations in Section VIII and in Section IX we examine the results, paying particular attention to whether or not there is an optimal value for the atom-light coupling parameter $\beta = NU_0/\kappa$. We also present results illustrating the dependence of the SNR on other system parameters such as the number of atoms and the intracavity lattice depth. We summarize our results and provide some perspective in Section X. We have also provided two appendices that give details omitted from the main text, including those of our numerical approach.

II. HAMILTONIAN AND EQUATIONS OF MOTION

Our system consists of a gas of N bosonic atoms inside a vertically oriented Fabry-Perot optical cavity. A single cavity mode of frequency ω_c is externally pumped by coherent laser light with a frequency ω_p that is detuned from the atomic resonance and the cavity resonance frequency. This sets up a standing wave mode along the cavity axis of the form $\cos(k_c z)$, where $k_c = \omega_c/c$. The relevant frequency relations are characterized by the two detunings

$$\Delta_c \equiv \omega_p - \omega_c, \quad (2a)$$

$$\Delta_a \equiv \omega_p - \omega_a, \quad (2b)$$

where ω_a is the atomic transition frequency. In the dispersive regime, the occupation of the excited atomic state is vanishingly small and it can be adiabatically eliminated. A one-dimensional hamiltonian for the atom-cavity system in the dispersive regime can then be written as [43, 44]

$$\begin{aligned} \hat{H} = & -\hbar\Delta_c\hat{a}^\dagger\hat{a} + i\hbar\eta(\hat{a}^\dagger - \hat{a}) \\ & + \int dz \hat{\Psi}^\dagger \left[-\frac{\hbar^2}{2M} \frac{\partial^2}{\partial z^2} + \hbar U_0 \hat{a}^\dagger \hat{a} \cos^2(k_c z) - Fz \right] \hat{\Psi}, \end{aligned} \quad (3)$$

where $\hat{\Psi}(z, t)$ and $\hat{a}(t)$ are the field operators for the atoms and the cavity photons which obey the equal time bosonic commutation relations $[\hat{\Psi}(x, t), \hat{\Psi}^\dagger(x', t)] = \delta(x - x')$, and $[\hat{a}(t), \hat{a}^\dagger(t)] = 1$, respectively. The single atom dispersive light shift has been denoted by $U_0 \equiv g_0^2/\Delta_a$.

The hamiltonian has been written in a frame rotating with the pump laser frequency ω_p , and this leads to the appearance of the two detunings. The first term is just the free evolution of the cavity mode. The second

term represents the laser coherently pumping the cavity at rate η , and the third term describes the atomic part of the hamiltonian. The first two terms of the atomic part represent the kinetic energy and a light induced potential energy. This latter term can either be understood as the atom moving in a periodic potential with average amplitude $\hbar U_0 \langle \hat{a}^\dagger \hat{a} \rangle$ or, if combined with the first term in the hamiltonian, as a shift in the resonance frequency of the cavity due to the coupling between the atom and the field. The third term in the atomic part provides the external force that drives the BOs. We assume this force arises from the vertical orientation (z increases in the downward direction) of the cavity and is given by $F = Mg$.

Note that we have not included direct atom-atom interactions. From a practical point of view this is because these are easily dwarfed by the atom-cavity interactions, or can be tuned away using a Feshbach resonance [46]. However, from a more pedagogical point of view, we want to focus here upon the nonlinearity which arises from atom-cavity interactions and avoid any confusion with the effects of direct atom-atom interactions which are in any case already well studied in quantum gases. The interactions between the atoms and the common light mode provided by the cavity gives rise to a nonlinearity that is in some ways analogous to the direct interactions but in other ways differs and can lead to novel behavior [43–45].

Natural units for the length and energy in cavity-QED are given by $1/k_c$ and the recoil energy $E_R = \hbar^2 k_c^2 / (2M)$, respectively. From here on we scale all lengths by $1/k_c$ and consequently define $x \equiv k_c z$. We scale frequencies by the recoil frequency $\omega_R \equiv E_R/\hbar$ and time by $1/\omega_R$ and retain the same symbols for the scaled variables. The Heisenberg-Langevin equations of motion for the light and atomic field operators in the scaled variables are [43]

$$i \frac{d\hat{a}}{dt} = \left[-\Delta_c + \int dx \hat{\Psi}^\dagger(x, t) \hat{\Psi}(x, t) U_0 \cos^2(x) - i\kappa \right] \hat{a} + i\eta + i\sqrt{2\kappa} \hat{\xi}(t) \quad (4a)$$

$$i \frac{\partial \hat{\Psi}}{\partial t} = \left[-\frac{\partial^2}{\partial x^2} + U_0 \hat{a}^\dagger \hat{a} \cos^2(x) - fx \right] \hat{\Psi} \quad (4b)$$

where $f \equiv F/(\hbar k_c \omega_R) = \omega_B/(\pi \omega_R)$ is the dimensionless form for the external force. The operator $\hat{\xi}(t)$ is the Langevin term and is assumed to be Gaussian white noise with the only non-zero correlation being

$$\langle \hat{\xi}(t) \hat{\xi}^\dagger(t') \rangle = \delta(t - t'). \quad (4c)$$

Mathematically, the Langevin noise terms are necessary in order to preserve the commutation relation $[\hat{a}(t), \hat{a}^\dagger(t)] = 1$ in an open system. Physically, their origin is vacuum fluctuations of the electromagnetic field that are transmitted into the cavity via the mirrors and they thus only appear in the equations for the light field. Nevertheless, the noise is conveyed to the atomic dynamics by the atom-light coupling.

III. MEANFIELD DYNAMICS: THEORY

The approach we follow in this paper is based upon a separation of the field operators into meanfield and quantum parts:

$$\hat{a}(t) = \alpha(t) + \delta\hat{a}(t) \quad (5a)$$

$$\hat{\Psi}(x, t) = \sqrt{N}\varphi(x, t) + \delta\hat{\Psi}(x, t). \quad (5b)$$

In the meanfield approximation the light is assumed to be in a classical state with amplitude $\alpha(t) = \langle\hat{a}(t)\rangle$, where $|\alpha(t)|^2$ corresponds to the average number of photons in the cavity, and the atoms are assumed to all share the same single-particle wave function $\varphi(x, t) = \langle\hat{\Psi}(x, t)\rangle/\sqrt{N}$. The equations of motion for the meanfield amplitudes $\alpha(t)$ and $\varphi(x, t)$ are

$$\begin{aligned} i\frac{d\alpha(t)}{dt} &= [-\Delta_c + NU_0\langle\cos^2(x)\rangle - i\kappa]\alpha(t) + i\eta \quad (6a) \\ i\frac{\partial\varphi(x, t)}{\partial t} &= \left[-\frac{\partial^2}{\partial x^2} + |\alpha(t)|^2U_0\cos^2(x) - fx\right]\varphi(x, t) \quad (6b) \end{aligned}$$

where the second equation has the form of a Schrödinger equation. The expectation value

$$\langle\cos^2(x)\rangle(t) = \int dx |\varphi(x, t)|^2 \cos^2(x) \quad (6c)$$

that appears in the first of these equations provides the time-dependent coupling between the atomic probability density and the cavity mode function. Multiplying this integral is the collective atom-cavity coupling parameter NU_0 . When measured in units of the cavity linewidth we denote this parameter by β

$$\beta \equiv NU_0/\kappa. \quad (7)$$

We illustrate the effect that β has on the meanfield dynamics in Figs. 2 and 3 below.

The time dependence of the meanfield amplitudes due to the BOs means that the coupled equations (6a) and (6b) already present a nontrivial problem [15]. However, in cold atom experiments there is often a large separation of time scales between the light and atom dynamics: the intrinsic dynamics of the light field is controlled by the size of Δ_c and κ , whereas the dynamics of the atomic meanfield is mainly determined by the period and depth $s(t) \equiv U_0|\alpha(t)|^2$ of the intracavity lattice. In the experiments [27, 28] the former is two or three orders of magnitude faster than the latter. Thus, on the time scales relevant to the slow atomic dynamics of the atoms, the light field relaxes to an instantaneous “steady state”

$$\alpha(t) \approx \frac{i\eta}{\Delta_c - NU_0\langle\cos^2(x)\rangle(t) + i\kappa}, \quad (8)$$

which simply tracks the instantaneous value of the atomic wave function $\varphi(x, t)$. This adiabatic elimination of the

dynamics of the light field results in a clear physical picture of the “classical” backaction referred to in the Introduction: As the atomic meanfield evolves in time the cavity light field is modulated due to the $\langle\cos^2(x)\rangle$ term in the denominator of Eq. (8) which in turn changes the amplitude of the light field in the cavity and hence the depth of the lattice potential that the atoms feel, and so on. Although the adiabatically eliminated form (8) is quite accurate in the regimes considered here, in our numerical calculations we nevertheless solve the full coupled equations (6a) and (6b).

In reference [32] we studied the influence the classical backaction nonlinearity has upon the band structure of atom-cavity systems. The band structure is given by the steady state solutions [$\dot{\alpha} = 0$, $\varphi(x, t) = \varphi(x)\exp(-i\mu t/\hbar)$] of the coupled equations of motion (6a) and (6b) in the absence of the external force f . It is straightforward to see that, despite the nonlinearity, exact solutions of the steady state problem are given by Mathieu functions (like in the linear problem a quantum particle in a fixed cosine potential). Mathieu functions are Bloch waves and so can be labelled by a band index b and quasimomentum q [47]

$$\varphi_{q,b}(x) = e^{iqx}\mathcal{U}_{q,b}(x) \quad (9)$$

where $\mathcal{U}_{q,b}(x + \pi) = \mathcal{U}_{q,b}(x)$ has the same period as the lattice. In the reduced zone picture q is restricted to lie in the first Brillouin zone $-1 < q \leq 1$. Substituting the Bloch wave solution into the equations of motion yields the steady state equations

$$\alpha_{ss} = \frac{i\eta}{\Delta_c - NU_0\langle\cos^2(x)\rangle + i\kappa} \quad (10a)$$

$$\mu_{q,b}\mathcal{U}_{q,b}(x) = \left[\left(-i\frac{\partial}{\partial x} + q\right)^2 + |\alpha_{ss}|^2U_0\cos^2(x)\right]\mathcal{U}_{q,b}(x) \quad (10b)$$

where the subscript ss denotes “steady state”. Solving these equations one obtains a *band structure* analogous to that in the linear case but with the striking difference that the nonlinearity can lead to swallowtail loops in the bands. It is important to appreciate that this band structure is not for the atoms alone, but for the combined atom-cavity system. For example, the eigenvalue μ is actually a chemical potential rather than the band energy (for the underlying energy functional with the light adiabatically eliminated see [32]), and another difference from the linear case is that the lattice depth $s = U_0|\alpha_{ss}|^2$ is not fixed, but instead depends on the values of $\{b, q\}$. So, for example, the lattice depth changes during a BO as q is swept along the band.

The external force f breaks the spatial periodicity and means that Bloch waves are replaced by Wannier-Stark states as the steady state solutions of the equations of motion (in fact, in any finite system the Wannier-Stark states are resonances rather than true eigenstates [48]). The spatial periodicity can be restored by applying

the unitary transformation $\bar{\varphi}(x, t) = \exp(-iftx)\varphi(x, t)$ which removes the fx term appearing in the hamiltonian in the Schrödinger equation (6b) and introduces a shift ft into the momentum operator

$$\begin{aligned} \mathcal{H} &= -\frac{\partial^2}{\partial x^2} + s(t) \cos^2(x) - fx \\ &\longrightarrow \bar{\mathcal{H}} = \left(-i\frac{\partial}{\partial x} + ft\right)^2 + s(t) \cos^2(x). \end{aligned} \quad (11)$$

We denote the frame resulting from this transformation as the transformed frame (TF), and the original frame as the lab frame (LF).

Let us now consider the dynamics under the influence of the force term. We take the initial atomic state $\bar{\varphi}(x, t=0) = \varphi(x, t=0)$ to be a Bloch state in the ground band with quasimomentum $q = q_0$. In the adiabatic approximation [49]

$$\bar{\varphi}(x, t) \approx \mathcal{U}_{q(t), b=0}(x) \exp\left[-(i/\hbar) \int_0^t dt' \mu_{q(t'), b=0}\right] \quad (12)$$

i.e. the atoms remain in the ground band but the force causes the quasimomentum to sweep periodically through the first Brillouin zone in accordance with the Bloch acceleration theorem

$$q(t) = q_0 + ft \quad (13)$$

as can be seen by comparing Eqns. (10b) and (11). In fact, a careful analysis [50] shows that Eq. (13) holds even when adiabaticity is broken and interband transitions are allowed providing these transitions are “vertical”, i.e. they conserve q .

This standard approach to BOs remains valid even when the lattice depth is modulated in time, as takes place in cavities, because amplitude modulation does not break the spatial periodicity of the potential and so cannot change q [15]. We therefore find that at any later time t , the *exact* atomic meanfield can be expressed as

$$\varphi(x, t) = \exp[i(q_0 + ft)x] \mathcal{U}(t). \quad (14)$$

In general $\mathcal{U}(t)$ is in a superposition of bands and so is no longer the steady state solution of Eqns. (10a) and (10b), although it does retain its Bloch form. The advantage of the TF is that the quasimomentum is frozen at its initial value and we have

$$\bar{\varphi}(x, t) = \exp[iq_0 x] \mathcal{U}(t) \quad (15)$$

so that it is only the spatially periodic function $\mathcal{U}(t)$ that evolves in time. From the point of view of numerical computation this allows us to work with a basis of periodic functions (we normalize our wave functions over one period of the lattice). At any given time a relatively small number of basis functions can accurately describe the atomic meanfield state and this greatly reduces the numerical effort in the calculation of BOs. Furthermore, since the quantum part of the field operators are also

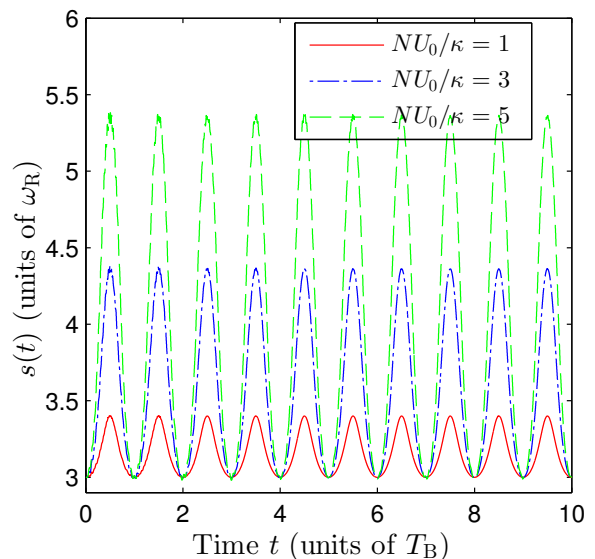


FIG. 2. (Color online) Intracavity optical lattice depth $s(t) \equiv U_0|\alpha(t)|^2$ in units of the atomic recoil frequency ω_R plotted as a function of time. The curves, which are each for a different value of the collective atom-cavity coupling parameter NU_0/κ , were obtained by solving the meanfield equations of motion Eqns. (6a) and (6b) and illustrate the fact that the change in lattice depth over one Bloch oscillation increases with NU_0/κ . In order to maintain a minimum lattice depth of $3E_R$ as NU_0/κ was increased by changing $U_0 = \{1, 3, 5\}u_0$, where $u_0 = 7 \times 10^{-3}\omega_R$, we also changed the pumping strength as $\eta = \{30.7, 24.2, 24.3\}\kappa$, giving mean photon numbers $\{458, 172, 117\}$, respectively. Other parameters for this plot are $\Delta_c = -0.75\kappa$, $\kappa = 345\omega_R$, and $N = 5 \times 10^4$. For all the plots in this paper the force is such that the Bloch frequency has the value $\omega_B = \omega_R/4$.

expanded in the same basis as the meanfield, the frame transformation also simplifies the numerical calculation of the quantum fluctuations as we detail in Section V.

By working in terms of Bloch waves rather than Wannier states, our approach is predisposed towards treating wave functions which are localized in momentum space rather than coordinate space. This choice is sensible because momentum space is a natural setting for BOs as is evident from Eq. (13). This is also in line with existing experiments demonstrating cold atom BOs in free space optical lattices [2, 6–9, 12, 13], where the initial state is generally a fairly narrow wavepacket in momentum space. In this paper we shall therefore restrict ourselves to states that are completely localised in quasimomentum (δ -function wave packet). Note that the inclusion of direct atom-atom interactions or an external trap will break the periodicity in Eq. (11) and induce “non-vertical scattering”, i.e. scattering between different quasimomentum states. Nevertheless, as explained in [41], in current experiments, e.g. [28], the periodicity breaking terms are quantitatively smaller and the essential features can be brought out by the approach we adopt.

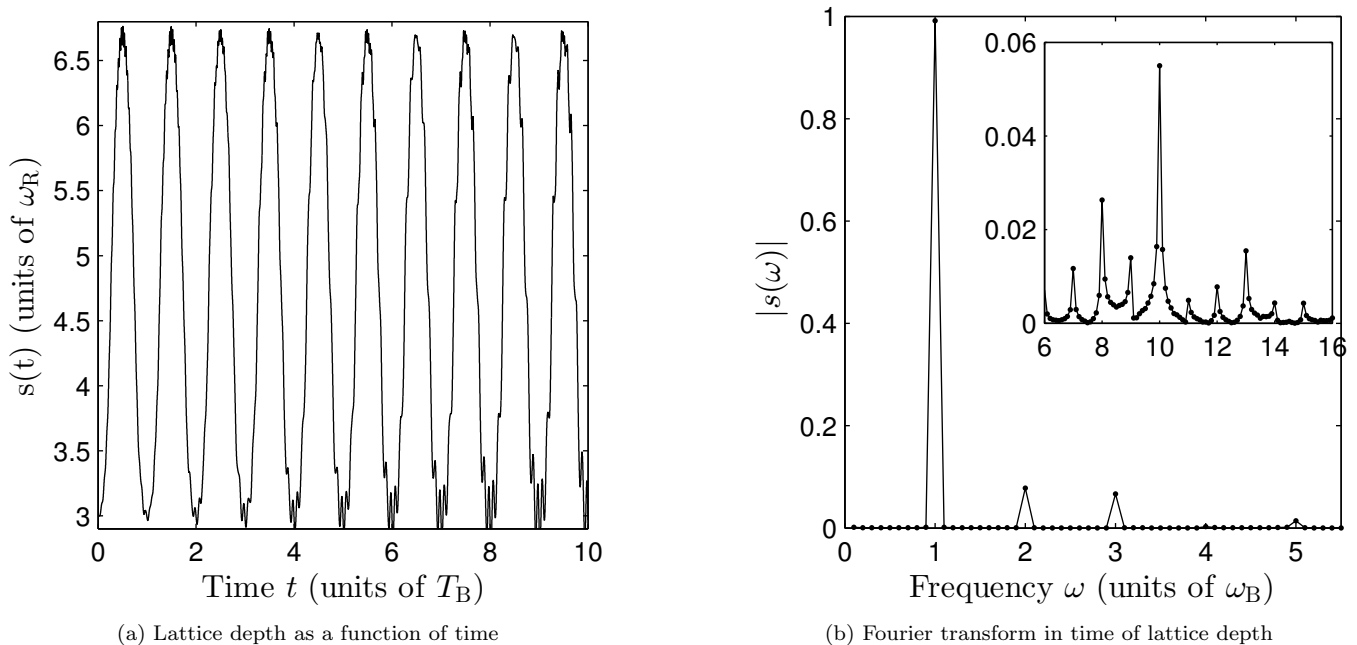


FIG. 3. The lattice depth $s(t)$ in units of the atomic recoil frequency ω_R is shown in (a) and its Fourier transform $s(\omega)$ is given in (b). We have increased the atom-cavity coupling from Fig. 2 to $NU_0/\kappa = 7.75$. At this larger value some fast fluctuations on top of the slow BO become visible. Their frequency is dominated by a harmonic at $10\omega_B$ as can be seen in the inset.

IV. MEANFIELD DYNAMICS: RESULTS

We now present our numerical results for the meanfield dynamics. The initial state at time $t = 0$ is taken to have quasimomentum $q = 0$, and be given by the solutions α_{ss} and $U_{0,0}(x)$ of the meanfield steady state equations [Eqns. (10a) and (10b)] for atoms in the ground band. This state is propagated in time using the meanfield equations of motion [Eq. (6a) and Eq. (6b)]. Our choices for the parameter values $\{U_0, N, \eta, \Delta_c, \kappa\}$ will be explained at the end of this Section.

Under the action of the external force the atoms begin performing BOs, which for atoms in extended Bloch states gives rise to a breathing motion of the atomic density distribution on each lattice site [15]. However, as explained in the Introduction, the atomic dynamics are not observed directly in the scheme considered here. Rather, the classical backaction [which is mediated by the atom-cavity coupling integral given in Eq. (6c)] imprints an oscillation on the amplitude and phase of the light field at the Bloch frequency ω_B as shown in Fig. 2 (what we actually plot in Fig. 2 is the the intracavity lattice depth $s(t) = U_0|\alpha(t)|^2$ seen by atoms, which is proportional to the number of cavity photons $|\alpha|^2$.) The experimental signature of the BOs is the photon current transmitted by the cavity, and this is given in the meanfield approximation by $\kappa \text{vert}\alpha(t)|^2$, and hence is directly proportional to $s(t)$.

The size of the backaction is controlled by the collective coupling $\beta = NU_0/\kappa$, as is apparent from the different

curves in Fig. 2. As β is increased the change in the lattice depth over a Bloch period increases and hence the visibility or *contrast* of the BOs as measured by a photon detector outside the cavity increases also. We define the contrast ϵ as

$$\epsilon \equiv (s_{\max} - s_{\min}) / (s_{\max} + s_{\min}). \quad (16)$$

Note that in the results shown in Fig. 2, each curve also has a different pumping strength η in order to maintain the same minimum lattice depth of $3E_R$. If the lattice becomes too shallow interband transition rates (e.g. due to Landau-Zener tunnelling around the band edges) become so high that the atoms effectively fall out of the lattice. On the other hand, if the lattice becomes too deep the contrast decreases (see Fig. 9a below and also Fig. 5 in [32]). A depth of $3E_R$ gives a reasonable compromise. Therefore, although in the rest of this paper we will examine the effects of changing the various system parameters, we will always maintain the minimum lattice depth at $3E_R$ (the one exception being in Fig. 9a). This also allows us to make comparisons between the effects of different parameter values upon, e.g. the quantum fluctuations, whilst keeping the atomic meanfield dynamics as similar as possible.

As the coupling β is increased other effects appear apart from an increase in the contrast. These effects are visible in Fig. 3 (see also Fig. 2 in [15]). In Fig. 3a we see that small-amplitude fast oscillations of the lattice depth appear on top of the basic BO. These fast oscillations have a frequency corresponding to the gaps between

bands and can therefore be associated with non-adiabatic effects, i.e. the excitation of higher bands [15]. This interpretation is consistent with the increase in amplitude of the fast oscillations with time that can be discerned in Fig. 3a. Referring to the Fourier transform of $s(t)$ plotted in Fig. 3b, we see that the basic BO dynamics is governed by the fundamental ω_B and its low lying harmonics, whereas the fast oscillations are clustered around the tenth harmonic (see inset) and include a continuum of frequencies with some peaks at half harmonics. In this context it is important to bear in mind that the band gaps change continuously in time as q is swept through the Brillouin zone and so a range of frequencies is to be expected.

The precision to which ω_B can be measured in the scheme proposed in this paper depends upon the contrast [15]. From the results shown in Fig. 2 it may therefore seem that in order to make the most sensitive measurement possible one should choose β to be as large as possible. However, this is false for two reasons. One is the effect of quantum fluctuations due to measurement back-action which is also controlled by β and will be the focus of Section VIII. Another reason, which enters even at the meanfield level, is the possibility of bistability in cavity photon number for large values of β (when the pumping is sufficiently large). In [28] this bistability was studied experimentally in a uniform unaccelerated condensate, which in our language has a quasimomentum $q = 0$. In [32] we studied this problem theoretically and generalized it to include finite q : we showed that bistability arises from the appearance of swallowtail loops in the bands. In the semiclassical picture of a BO the quasimomentum scans adiabatically through the entire band and so when it encounters a swallowtail loop the system can follow a branch that suddenly terminates at some later time, leading to fundamentally nonadiabatic behavior [15, 51]. Hence, in a scheme to measure BOs, it would be better to be in a parameter regime where the cavity is not bistable for any value of q . In Fig. 4 we plot the pump strength required to maintain the lattice depth at a minimum value of $3E_R$ as a function of β . The red (solid) and blue (dot-dashed) lines enclose the values of η for which the steady state photon number in the cavity displays bistability for at least some values of the quasimomentum. We see that for β values as large as 25 (at the fixed detuning $\Delta_c = -0.75\kappa$) one can avoid bistability and get large contrast in the lattice depth evolution.

Having emphasized that our choice for the pumping strength η is guided by the tradeoff between contrast and bistability according to Fig. 4, let us now explain how we chose the rest of the system parameters used in the calculations. There are three parameters we hold constant throughout this paper; the first is the cavity damping rate $\kappa = 345\omega_R$ which is the value realized in the experiment [28]. As a guide to the magnitude of the atomic recoil frequency ω_R used as the frequency unit, we note that for ^{87}Rb atoms in 780nm light $\omega_R = 2\pi \times 3.8$ kHz. The second constant parameter is the Bloch fre-

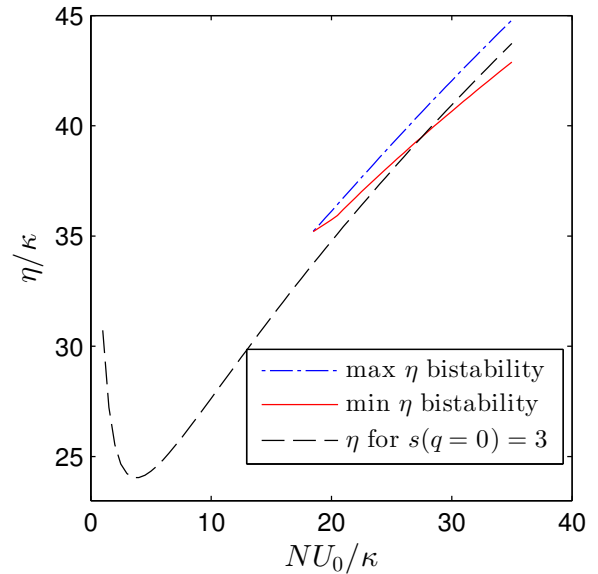


FIG. 4. (Color online) Plot of pump strength (dashed black line) required to maintain a minimum lattice depth of $3E_R$ as a function of NU_0/κ . The red (solid) and blue (dash-dotted) lines enclose the values of η for which the steady state photon number in the cavity is bistable for any value of the quasimomentum of the atomic wave function. One sees that for $NU_0/\kappa \sim 25$, the pump strength required to maintain the lattice depth leads to bistability. Other parameters for the plot are $\Delta_c = -0.75\kappa$, $\kappa = 345\omega_R$, $N = 5 \times 10^4$

quency $\omega_B = \omega_R/4$. The gravitational force on ^{87}Rb atoms in a 780nm lattice provides a Bloch frequency very close to this value. Finally, unless specified otherwise, we keep the meanfield atom number fixed at $N = 5 \times 10^4$ and vary U_0 in order to vary β . This last choice is motivated by a scaling symmetry of the meanfield equations [Eqns. (6a)-(6b)], which also holds for the quantum operator equations [Eqns. (24a)-(24b)] below; solving the coupled equations for the set of parameters $\{U_0, N, \eta, \Delta_c, \kappa\}$ is exactly the same as solving them for $\{U_0 r, N/r, \eta/\sqrt{r}, \Delta_c, \kappa\}$, where r is some positive scaling factor. In both the scaled and unscaled versions the lattice depth $s(t) = U_0|\alpha(t)|^2$ is maintained at the same value. Thus, each specific calculation one performs represents a family of parameters. Our choice for N keeps the atomic density dilute enough in a typically sized cavity that the approximation of ignoring collisional atom-atom interactions remains valid. There is some latitude in the choice of Δ_c , but the contrast one obtains at a given value of β is larger for Δ_c closer to the cavity resonance. On the other hand, one also has to make sure that the effective cavity detuning

$$\Delta_c^{\text{eff}} \equiv \Delta_c - NU_0\langle\cos^2(x)\rangle \quad (17)$$

is less than zero so that we are in the cavity cooling regime for the fluctuations [40] (see Section VI). We set $\Delta_c = -0.75\kappa$ since we find that it maximizes the contrast

for the coupling value of $NU_0/\kappa = 1$. We will examine the effect of changing the number of atoms N and the minimum lattice depth when we examine the signal-to-noise ratio in Section VIII.

V. QUANTUM DYNAMICS: THEORY

The approach we take to quantum dynamics is based upon a linearization about the meanfield solution, retaining the quantum operators $\delta\hat{a}$ and $\delta\hat{\Psi}$ only to first order in the equations of motion. This corresponds to the Bogoliubov level of approximation [52, 53], suitably generalized to describe coupled atomic and light fields. A new feature of our problem in comparison to previous linearization-based treatments of cavity-QED systems, e.g. [39, 41, 42], is that our meanfield is time-dependent because of the BOs. This means that the fluctuation modes, which must be orthogonal to the meanfield mode, also evolve in time (not just their occupations).

Linearizing about the meanfield solution may appear to be an innocent strategy, but, as is well known from the theory of Bose-Einstein condensation, care must be taken with such U(1) symmetry breaking approaches because they introduce a macroscopic (meanfield) wave function with a particular global phase at the cost of particle number conservation [54]. In particular, when performing a linearization about the condensate there is always a trivial fluctuation mode parallel to it with zero frequency (the “zero mode”) which corresponds to unphysical fluctuations of the global phase. These issues are even more acute when the condensate is time-dependent and the boundary between condensate and fluctuation is further blurred [55].

The zero mode problem can be handled by only including fluctuations that are at all times orthogonal to the meanfield. We achieve this by applying the projector $\hat{P}(t)$ [55, 56]

$$\hat{P}(t) = \mathcal{I} - |\varphi(t)\rangle\langle\varphi(t)| \quad (18)$$

so that

$$\begin{aligned} \delta\hat{\Psi}_\perp(x, t) &\equiv \hat{P}\delta\hat{\Psi}(x, t) \\ &= \int dy [\delta(x - y) - \varphi(x, t)\varphi^*(y, t)] \delta\hat{\Psi}(y, t). \end{aligned} \quad (19)$$

One consequence of this is that the commutator between atomic fluctuations is given by [57]

$$\begin{aligned} [\delta\hat{\Psi}_\perp(x, t), \delta\hat{\Psi}_\perp^\dagger(y, t)] &= \langle x | \hat{P}(t) | y \rangle \\ &= \delta(x - y) - \varphi(x, t)\varphi^*(y, t). \end{aligned} \quad (20)$$

Unlike the usual bosonic commutator for the fluctuation field $\delta\hat{\Psi}$, this is time dependent.

Next, we transform the atomic fluctuation operator from the LF to the TF

$$\bar{\delta\hat{\Psi}}(x, t) = \delta\hat{\Psi}(x, t)e^{-iftx}. \quad (21)$$

This simplifies the calculation for the same reasons as mentioned in Section III for the meanfield. Since only “vertical” fluctuations between bands can occur, both the fluctuations and the meanfield have the same quasimomentum, which in the TF is frozen at its initial value. This allows us to expand the fluctuations and meanfield in the same basis

$$\bar{\varphi}(x, t) = \sum_n c_n e^{i2nx} \quad (22)$$

$$\bar{\delta\hat{\Psi}}_\perp(x, t) = \sum_n \delta\hat{c}_n e^{i2nx}. \quad (23)$$

where we have set the initial quasimomentum $q_0 = 0$ without loss of generality. Meanwhile, back in the LF, the quasimomentum evolves according to the Bloch acceleration theorem given by Eq. (13).

We can now write down the coupled equations of motion for the fluctuation operators as

$$i\frac{d}{dt}\delta\hat{a}(t) = A(t)\delta\hat{a}(t) + \sqrt{N}U_0\alpha(t) \int dx \cos^2(x) [\bar{\varphi}^*(x, t)\bar{\delta\hat{\Psi}}_\perp(x, t) + \bar{\varphi}(x, t)\bar{\delta\hat{\Psi}}_\perp^\dagger(x, t)] + i\sqrt{2\kappa}\hat{\xi}(t) \quad (24a)$$

$$i\frac{\partial}{\partial t}\bar{\delta\hat{\Psi}}_\perp(x, t) = \bar{\mathcal{H}}(t)\bar{\delta\hat{\Psi}}_\perp(x, t) + \sqrt{N}U_0\hat{P}(t)\cos^2(x)\bar{\varphi}(x, t) [\alpha^*(t)\delta\hat{a}(t) + \alpha(t)\delta\hat{a}^\dagger(t)] \quad (24b)$$

where $A(t) \equiv (-\Delta_c + NU_0\langle\cos^2(x)\rangle(t) - i\kappa)$. The structure of these equations is such that if initially $\delta\hat{a} = \bar{\delta\hat{\Psi}}_\perp = 0$ then in the absence of the Langevin terms these quantum parts of the fields would remain zero for all time. The Langevin fluctuations appear as an inhomogeneous term in the cavity field equation and act as a source that drives the growth of $\delta\hat{a}$ which in turn drives

the growth of $\bar{\delta\hat{\Psi}}_\perp$ via the atom-cavity coupling.

As pointed out in [41], the dynamics of the complex valued operators in the above equations can be solved either by separating out their real and imaginary parts (optomechanics approach) or by simultaneously solving the equations for the hermitian conjugates of the operators (the Bogoliubov-de Gennes approach). We choose the latter. Collecting the fluctuations into the column

vector $\hat{R}(t) = (\delta\hat{a}, \delta\hat{a}^\dagger, \delta\hat{\Psi}_\perp, \delta\hat{\Psi}_\perp^\dagger)^T$, and the noise operators that act as source terms into the column vector $\hat{Z}(t) = \sqrt{2\kappa}(\hat{\xi}, \hat{\xi}^\dagger, 0, 0)^T$, where T denotes transposition,

we obtain the operator matrix equation

$$i\frac{\partial}{\partial t}\hat{R} = \mathbf{M}\hat{R}(t) + i\hat{Z}(t) \quad (25a)$$

with

$$\mathbf{M}(t) = \begin{bmatrix} A & 0 & \sqrt{N}U_0\alpha V^* & \sqrt{N}U_0\alpha V \\ 0 & -A^* & -\sqrt{N}U_0\alpha^* V^* & -\sqrt{N}U_0\alpha^* V \\ \sqrt{N}U_0\alpha^* W(x) & \sqrt{N}U_0\alpha W(x) & \hat{P} \bar{\mathcal{H}}(t) & 0 \\ -\sqrt{N}U_0\alpha^* W^\dagger(x) & -\sqrt{N}U_0\alpha W^\dagger(x) & 0 & -\hat{P}^\dagger \bar{\mathcal{H}}(t) \end{bmatrix} \quad (25b)$$

where we have introduced the operators

$$V \cdot g(x) \equiv \int dx \bar{\varphi}(x, t) \cos^2(x) g(x) \quad (25c)$$

$$W(x) \equiv \hat{P} \cos^2(x) \bar{\varphi}(x, t) \quad (25d)$$

i.e. V is an integral operator that acts on a function $g(x)$. Since they fall on the off-diagonals, the terms involving V and W couple the cavity and atom fluctuations. Observe, however, that in the linear approximation used here the atomic fluctuation operators $\delta\hat{\Psi}_\perp(x, t)$ are not directly coupled to the cavity fluctuation operators $\delta\hat{a}(t)$ because this would lead to terms which are of second order. Rather, the coupling between the two sets of quantum fields is mediated by the meanfields $\alpha(t)$ and $\bar{\varphi}(x, t)$.

The matrix $\mathbf{M}(t)$ is non-normal, i.e. it does not commute with its Hermitian adjoint and its left and right eigenvectors are not the same. However, it does have the following symmetry property: a linear transformation \mathcal{T} that swaps the first and second, and simultaneously, the third and fourth rows, produces a matrix which is proportional to the complex conjugate of the original [40]

$$\mathcal{T} \cdot \mathbf{M} \cdot \mathcal{T} = -\mathbf{M}^*. \quad (26)$$

This symmetry, which is a general feature of Bogoliubov-de Gennes type equations [11], implies that the eigenvalues (and the associated eigenvectors) occur in pairs of the form $\pm\omega_n + i\gamma_n$ i.e. with the same imaginary parts but with real parts of opposite sign. We shall explore the spectrum of the fluctuation matrix \mathbf{M} further in the Section VI. We also note that when written in matrix form the role of the projection operator becomes clear since one can immediately see that the vectors $(0, 0, \bar{\varphi}(x, t), 0)^T$ and $(0, 0, 0, \bar{\varphi}^*(x, t))^T$ span the zero eigenvalue subspace of the matrix \mathbf{M} and the trivial fluctuations live in this subspace.

The time evolution of the fluctuation operators is given by solving Eq. (25a). However, measurable observables are given by expectation values and correlation functions of these operators rather than by the operators themselves. To this end we consider the covariance matrix

$\mathbf{C}(t)$ associated with the vector \hat{R}

$$\mathbf{C}_{jk}(t) \equiv \langle \hat{R}_j \hat{R}_k \rangle(t). \quad (27)$$

Particular cases of $\mathbf{C}_{jk}(t)$ include the total number of photonic and atomic fluctuations

$$\delta n(t) = \langle \delta\hat{a}^\dagger(t) \delta\hat{a}(t) \rangle \quad (28)$$

$$\delta N(t) = \int dx \langle \delta\hat{\Psi}_\perp^\dagger(x, t) \delta\hat{\Psi}_\perp(x, t) \rangle. \quad (29)$$

The latter correspond to the number of atoms excited out of the meanfield component (i.e. the atomic depletion).

To obtain the time evolution of the covariance matrix, consider the formal solution to Eq. (25) [58]

$$\hat{R}(t) = \mathbf{G}(t, 0) \hat{R}(0) + \mathbf{G}(t, 0) \int_0^t \mathbf{G}^{-1}(\tau, 0) \hat{Z}(\tau) d\tau \quad (30)$$

where $\mathbf{G}(t)$ is a matrix satisfying:

$$\dot{\mathbf{G}}(t, 0) = -i\mathbf{M}(t, 0)\mathbf{G}(t, 0); \quad \mathbf{G}(0, 0) = \mathcal{I}. \quad (31)$$

We drop the dependence of \mathbf{G} on the initial time for notational convenience in what follows. Inserting this formal solution in Eq. (27) we find

$$\mathbf{C}(t) = \mathbf{G}(t)\mathbf{C}(0)\mathbf{G}^T(t) + \mathbf{G}(t)\Sigma(t)\mathbf{G}^T(t) \quad (32)$$

$$\Sigma(t) \equiv \int_0^t \int_0^t \mathbf{G}^{-1}(\tau) \langle \hat{Z}(\tau) \hat{Z}(\tau') \rangle [\mathbf{G}^{-1}(\tau')]^T d\tau d\tau'. \quad (33)$$

Using the property of the Langevin noise terms given in Eq. (4c), we can simplify $\Sigma(t)$ as

$$\Sigma(t) = \int_0^t \mathbf{G}^{-1}(\tau) D[\mathbf{G}^{-1}(\tau)]^T d\tau \quad (34a)$$

$$D_{jk} \equiv 2\kappa\delta_{j1}\delta_{k2}. \quad (34b)$$

Our main numerical task is thus to solve the matrix differential equation given by Eq. (31). In addition, the matrix elements of $\mathbf{M}(t)$ have to be computed from the

meanfields $\{\alpha(t), \bar{\varphi}(x, t)\}$ obtained by solving the coupled equations Eq. (6a) and Eq. (6b). These latter equations are simply a set of ordinary differential equations that we solve using an adaptive time-step Runge-Kutta scheme. We then solve the matrix differential equation for $\mathbf{G}(t)$ using the same time grid as the meanfield solution. For the matrix differential equation, and the associated solution for the covariance matrix $\mathbf{C}(t)$, we can again use a Runge-Kutta algorithm or exponentiate the fluctuation matrix $\mathbf{M}(t)$ over the (small) time step intervals [59].

As a check on the results we can use the fact that the elements of the covariance matrix $\mathbf{C}(t)$ have to obey the commutator relations Eq. (20) for the operators making up $\hat{R}(t)$. For example, when the atomic operator is expanded as in Eq. (22), the expectation value of the commutator relation Eq. (20) gives

$$\langle \delta \hat{c}_n \delta \hat{c}_m^\dagger \rangle - \langle \delta \hat{c}_m^\dagger \delta \hat{c}_n \rangle = \delta_{nm} - \langle n | \bar{\varphi}(t) \rangle \langle \bar{\varphi}(t) | m \rangle. \quad (35)$$

The left hand side of this equation gives the difference between certain entries of the covariance matrix and we can calculate its expected value (the right hand side) from the meanfield solution. The degree of agreement between the two sides provides a measure of the accuracy of the fluctuation calculation. In general, we find that the accuracy can be increased by taking smaller time steps.

In closing this section, we would like to point out that the meanfield solution already includes Landau-Zener type tunnelling that causes the *coherent* excitation of higher bands. By contrast, the effect of Langevin fluctuations ξ is to *incoherently* populate different bands. Within the linear approximation used here, the depletion of the atomic meanfield by quantum excitations is not self-consistent, i.e. the meanfield is always normalized to N atoms, whatever the number of depleted atoms δN . The linearized equations used here are clearly only valid when $\delta N \ll N$, as expected from a Bogoliubov-type approach.

VI. SPECTRUM OF ELEMENTARY EXCITATIONS

Before presenting the results of the combined meanfield and quantum dynamics (see the next section), we shall first examine the excitation spectrum of the atom-cavity system. The excitation spectrum gives insights into the dynamics and will also be of use in explaining resonances that strongly affect the signal-to-noise ratio of the Bloch frequency measurement, a topic we will discuss in Section IX.

We first note that there are two distinct types of excitation, and hence spectra. The coupled atom-cavity band structure discussed in Section III refers to meanfield excitations which are labelled by a band index and a quasimomentum. They involve every atom and photon responding identically since, by the nature of the meanfield approximation, they are assumed to be described

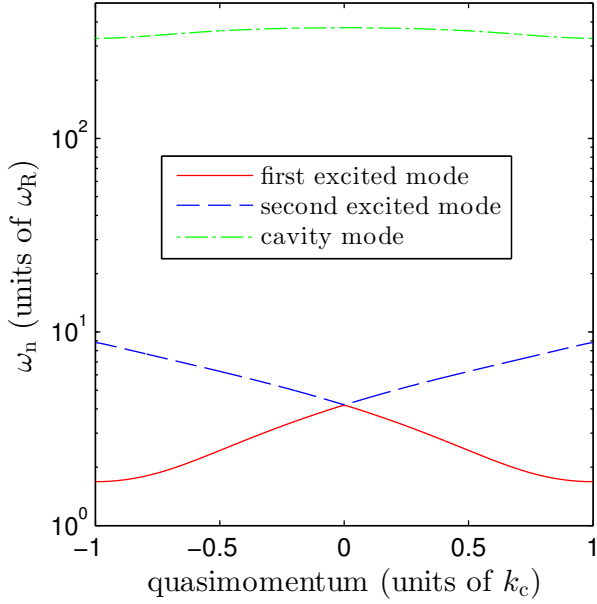
by a single wave function $\varphi(x, t)$ and the coherent amplitude $\alpha(t)$, respectively. On top of these, there are also elementary excitations or quasiparticles whose energies are the complex eigenvalues $\pm\omega_n + i\gamma_n$ of the matrix $\mathbf{M}(t)$ given in Eq. (25b). A clear description of the difference between the meanfield and the quasiparticle spectra for a BEC in a (non-cavity) optical lattice can be found in [60] and references therein. In the atom-cavity system the quasiparticles correspond to single quanta of the combined fields and are thus *polaritons*. The fact that they come in pairs can be interpreted as an analogue of particles and antiparticles [11].

Whereas the meanfield band structure is always real, the quasiparticle energies have an imaginary part which comes from the leaking of the cavity field out of the cavity. If $\gamma_n < 0$, we have dynamical stability and $|\gamma_n|$ can be interpreted as the lifetime of the quasiparticle. This damping effect has potentially very important applications in cavity-assisted cooling [39, 61]. If, on the other hand, $\gamma_n > 0$ we have dynamical instability and heating.

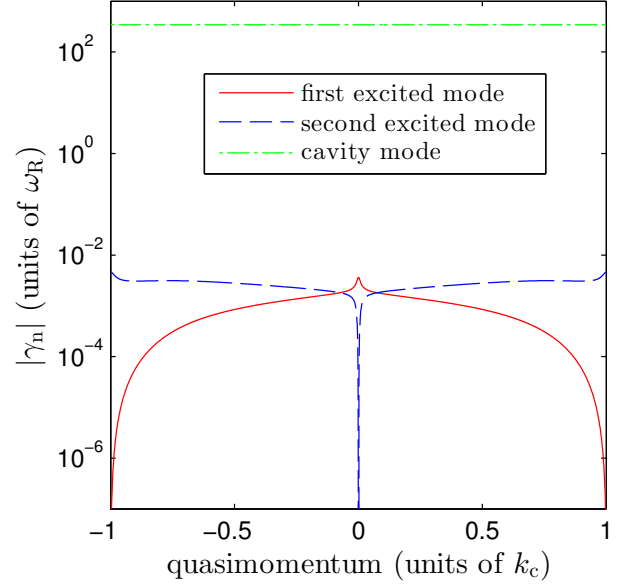
In general, the elementary excitations have a band structure all of their own, i.e. the solutions of the Bogoliubov-de Gennes equations take the form of Bloch waves with a band index and quasimomentum that can differ from that of the meanfield solution about which we are linearizing. However, as discussed in Section III, here we only allow excitations that preserve the quasimomentum (vertical transitions), and thus our quasiparticles have the same quasimomentum as their parent meanfield solution. Some examples are plotted as a function of quasimomentum in Fig. 5. We note in passing that there is in fact no need to quantize the fluctuations $\delta\Psi$ and $\delta\alpha$ about the meanfield in order to obtain \mathbf{M} . Thus, the spectrum of elementary excitations can also be obtained by considering classical fluctuations about the meanfields. This is well known in the case of BECs, where the linearized Gross-Pitaevskii equation (the meanfield equation of motion) gives the Bogoliubov spectrum. The truly quantum part of the dynamics here comes from the Langevin fluctuation operators $\hat{\xi}(t)$.

The eigenvectors of \mathbf{M} can be roughly classified into three kinds: cavity-like modes, hybridised atom-cavity modes, and marginally stable modes [40]. The cavity-like modes (depicted by the green dash-dotted lines in Fig. 5) are close to being pure cavity field modes with only a small atomic component. Hence, their eigenvalues have a real part with magnitude close to the effective detuning $\Delta_c^{\text{eff}} = \Delta_c - NU_0 \langle \cos^2(x) \rangle$, and an imaginary part approximately equal to $-\kappa$. The hybridized modes (depicted by the red solid and blue dashed lines in Fig. 5) have some atomic and some cavity field properties, whereas the marginally stable modes are purely atomic in nature with zero cavity component. As we shall demonstrate below, the marginally stable modes occur at the points $q = 0$ and $q = \pm 1$, i.e. at the band center and edges, and their name derives from the fact that their imaginary part is zero.

The properties of the hybridised and marginally stable



(a) Real part of the quasiparticle spectrum as a function of quasimomentum



(b) Imaginary part of the quasiparticle spectrum as a function of quasimomentum

FIG. 5. (Color online) Low lying levels in the quasiparticle spectrum (elementary excitations). The frequency of the n th level is generally complex $\omega_n + i\gamma_n$. The parameters used in the plots are $U_0 = 0.01 \omega_R$, $\kappa = 345 \omega_R$, $\Delta_c = -0.75 \kappa$, and $N = 5 \times 10^4$. The red (solid) and blue (dotted) lines correspond to hybridised atom-cavity modes and generally have non-zero imaginary parts except at certain special points such as at the band center and edges where they can become marginally stable and decouple from the cavity. The green (dash dotted) line corresponds to a cavity-like mode, i.e. the real part of its frequency is close to the effective detuning frequency $\Delta_c^{\text{eff}}(q)$, and the imaginary part is close to $-\kappa$.

modes are determined by the sign of Δ_c^{eff} . When $\Delta_c^{\text{eff}} < 0$ we find $\gamma_n < 0$ and we are on the cooling side of the effective resonance. On the contrary, when $\Delta_c^{\text{eff}} > 0$ we find $\gamma_n > 0$ and we are on the heating side. A calculation of the dynamics on the heating side is not stable since the linearisation will fail after a short time due to the exponentially growing number of quasiparticles. Thus, the calculation of the spectra serves a very useful purpose: it guides our choice of Δ_c so as to ensure that we are always on the cooling side of the resonance.

In Fig. 5a the red (solid) and blue (dashed) lines give the magnitudes of the real parts of the frequencies of the two lowest eigenmodes as a function of quasimomentum. The magnitudes of the imaginary parts are plotted in Fig. 5b. Notice that the imaginary part of one of the modes goes to zero at the band edges (red solid line) and the other goes to zero at the band center (blue dashed line). This implies that these excitations are only marginally stable at those specific values of the quasimomentum. The vanishing of the imaginary part of the frequencies at these points can be understood as follows: a Bloch wave with $q = 0$ ($q = 1$) is even (odd) about the center of a single cell $[0, \pi]$ of the $\cos^2(x)$ potential. Since the atomic meanfield solution $\bar{\varphi}(x)$ is a Bloch wave it has well defined parity at these points. The same is also true for the eigenmodes $\delta\hat{\Psi}_\perp(x)$ of the fluctuation matrix \mathbf{M} , for these are also Bloch waves. In this case the integral

$\int dx \bar{\varphi}^*(x) \cos^2(x) \delta\hat{\Psi}_\perp(x)$ will sometimes vanish identically because the integrand can contain functions with opposite parity. Examination of the fluctuation matrix \mathbf{M} given in Eq. (25b) shows that it is exactly this integral that controls the weight of the cavity part of the quasiparticle eigenmode, and so at $q = 0, \pm 1$ we can have undamped quasiparticles with $\gamma = 0$. For nonzero values of quasimomentum the meanfield wave function has no particular parity and there are no marginal modes.

VII. QUANTUM DYNAMICS: RESULTS

In this section we present results from the numerical solution of the quantum equations of motion. We assume that at $t = 0$ the fluctuation fields $\delta\hat{a}$ and $\delta\hat{\Psi}_\perp$ are in their vacuum states and expand the atomic part in the basis given in Eq. (23). This allows us to construct the covariance matrix Eq. (27) $\mathbf{C}(t = 0)$ which we then evolve to later times using Eq. (31). In order to perform this task we need the fluctuation matrix $\mathbf{M}(t)$ as a function of time which in turn requires the meanfield solution $\{\bar{\varphi}(x, t), \alpha(t)\}$ as input. We must therefore solve the meanfield dynamics on the same discretized time grid in parallel to the computation of Eq. (31). Once we have computed $\mathbf{C}(t)$, we can extract the various physical quantities of interest from it.

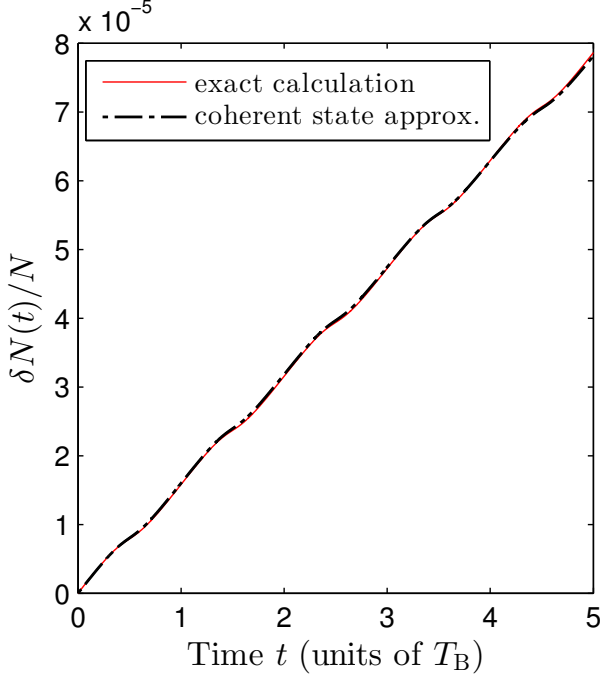
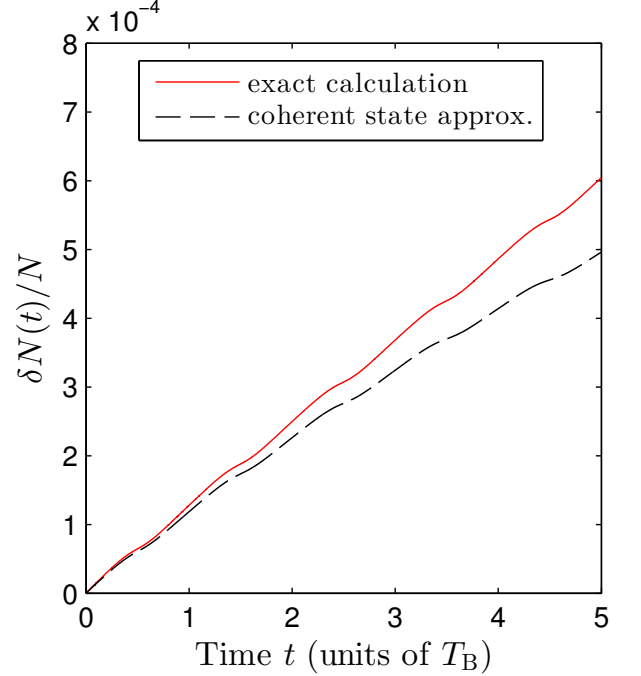
(a) Excited atom fraction versus time for $NU_0/\kappa = 0.1$ (b) Excited atom fraction versus time for $NU_0/\kappa = 1$

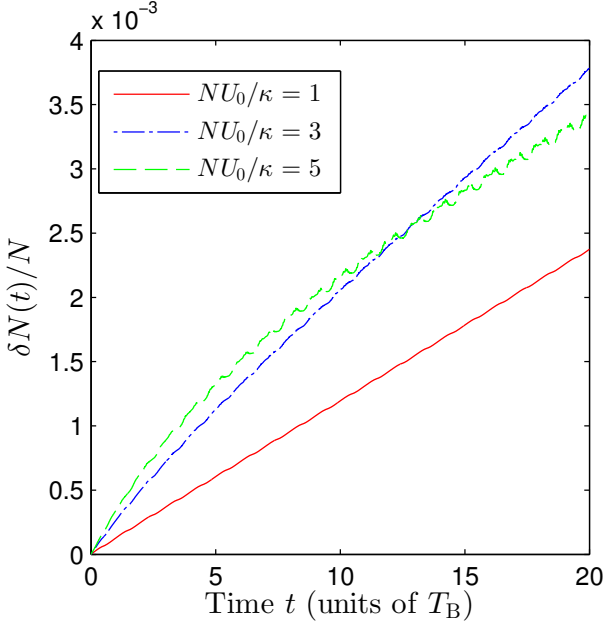
FIG. 6. (Color online) Growth of the excited atom fraction over five BO periods for weak (a) and moderately strong (b) atom-cavity coupling. The red (solid) curves are given by solving the full quantum problem in the form of Eq. (31), whereas the black (dashed) curves are the result of making the approximation that the quantum fluctuations come purely from vacuum shot noise, i.e. the coherent state approximation. The meanfield dynamics for (b) is given by the red (solid) curve in Fig. 2.

One such quantity is the number of atomic excitations δN , which is defined in Eq. (29). This should not be confused with the number of quasiparticles because the latter are generally made up of both atomic and cavity field components. If it were not for the Langevin noise, the evolution would be perfectly coherent and δN would be zero. However, the presence of Langevin noise in the electromagnetic field generates atomic excitations via the atom-cavity coupling. In Fig. 6 we plot the fraction $\delta N(t)/N$ as a function of time for five Bloch periods for two different coupling values. The red (solid) curves are given by a full solution of the quantum equations, whereas the black (dashed) curves are made with a coherent state approximation for the cavity field, which will be outlined below and is discussed in more detail in Appendix A. The gradient of these curves gives the heating rate and over five BOs this appears to be roughly linear. However, over longer times the number of atoms (and photons) excited out of the meanfield begins to saturate, as shown in Fig. 7. The saturation occurs because on the cooling side of the effective resonance, where $\Delta_c^{\text{eff}} < 0$, there is a competition between the heating due to the Langevin noise \hat{Z} and the dynamical stability of \mathbf{M} leading to nonzero but finite values of δN at long times.

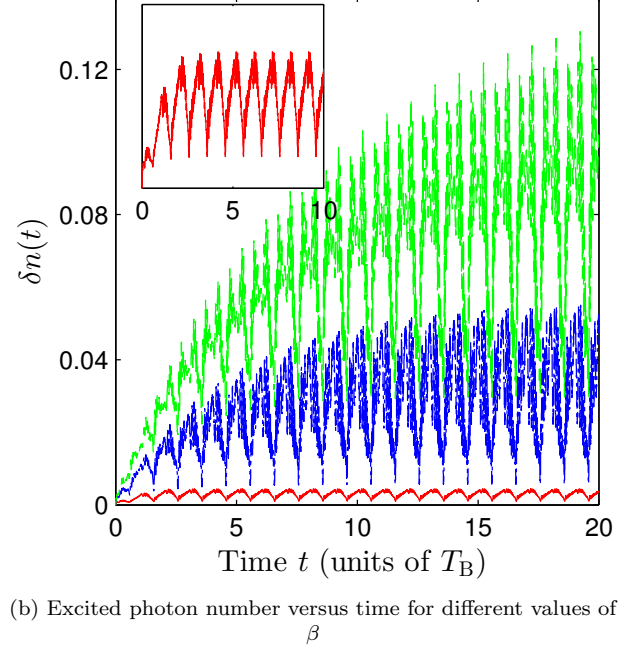
Superimposed upon the steady growth of the number of atomic excitations shown in Fig. 6, it is possible discern small modulations with a period equal to that of a BO.

These modulations are much more evident in the photon dynamics shown in Fig. 7b. They are due to the oscillation of the atom-cavity coupling during a BO, which takes its greatest value at $q = 0$ and its smallest value at $q = \pm 1$. Indeed, close examination of the modulations in Fig. 6 reveals that the heating rate at the zone edges is lower than at the zone center (recall that the initial condition is $q = 0$ at $t = 0$, and the system returns to this point after time T_B : at time $T_B/2$, the system is at the edge of the Brillouin zone). The coupling integrals enter \mathbf{M} , and referring to Fig. 5, we that this effect manifests itself in the dependence of the quasiparticle mode energies upon q : at the zone edges the quasiparticle mode with the smallest real part (red solid curve) becomes marginally stable, i.e. the cavity light field part and the atomic part decouple. This means that close to the zone edge new quasiparticles can only be created in a mode with higher energy (blue dotted line) which leads to a lowering of the heating rate.

In order to gain further insight into the fluctuation dynamics, let us develop a simple approximate model which we will call the “coherent state approximation” that assumes that the cavity field is described by a Glauber coherent state. This is a quantum state that has the same fluctuations as the vacuum and so neglects the fluctuation correlations that develop between the atoms and cavity field. Consider the exact solution to the first or-



(a) Excited atom fraction versus time for different values of β .



(b) Excited photon number versus time for different values of β .

FIG. 7. (Color online) Plots of atomic (a) and photonic (b) fluctuation occupation number over 20 BOs calculated using a numerical solution of Eq. (31). In (b) the lowest curve (red) is for $\beta = 1$, the middle curve is for $\beta = 3$ and the highest curve is for $\beta = 5$. Note the saturation in the growth rate, which is especially obvious in the photons. The inset in (b) shows a close up of the photonic fluctuation number as a function of time for $\beta = 1$. It can be seen how after a transient period the photonic fluctuation number oscillates at the Bloch period, thereby mirroring the meanfield dynamics.

der inhomogeneous differential equation for cavity field fluctuations Eq. (24a), which can be formally written as

$$\delta\hat{a}(t) = e^{-i\int_0^t dt' A(t')} \times \int_0^t dt' e^{i\int_0^{t'} dt'' A(t'')} [\sqrt{2\kappa}\hat{\xi}(t') - i\sqrt{N}U_0\alpha(t')\hat{X}(t')] \quad (36)$$

where $\hat{X}(t) \equiv \int dx \bar{\varphi}^*(x, t) \cos^2(x) \delta\bar{\Psi}_\perp(t) + \text{h.c.}$, and $A(t) = -\Delta_c^{\text{eff}}(t) - i\kappa$, as above. From Eq. (36) we see that the cavity field fluctuation has two distinct contributions: the first term depends on the Langevin noise which accounts for vacuum fluctuations, whilst the second term depends on the state of the atoms. The coherent state approximation consists of dropping the latter term in favour of the former to give

$$\delta\hat{a}(t) \approx \sqrt{2\kappa} \int_0^t dt' e^{i(\Delta_c^{\text{eff}}(t) - \kappa)(t-t')} \hat{\xi}(t'). \quad (37)$$

In writing $\delta\hat{a}(t)$ in this way we have taken advantage of the fact that the cavity decay rate κ is much faster than the frequency ω_B at which $\Delta_c^{\text{eff}}(t)$ evolves, and so the integrand is appreciable only for times $t - t' \lesssim \kappa^{-1}$ during which Δ_c^{eff} is a constant and can be evaluated at time t .

The regime of validity of the coherent state approximation can be estimated from its derivation which requires $r \equiv \sqrt{N}U_0|\alpha(t)|/\sqrt{2\kappa} \ll 1$. Note that $r^2 = \beta s(t)/2$.

In our earlier discussion (Section IV) of desirable parameters, we stipulated a minimum lattice depth of $s(t) \sim 3\omega_R$, which implies that the validity of the coherent state approximation here is contingent upon $\beta \ll 1$, i.e. this is a weak coupling approximation.

A measure of the magnitude of the correlations between the atomic and cavity field excitations, i.e. the degree to which the cavity field differs from a coherent state, can be seen in the difference between the red solid and black dashed curves in Fig. 6 for $\delta N(t)/N$. The latter neglects these correlations. We can thus infer that when $\beta = 0.1$ the correlations are small, but when $\beta = 1$ their effect is noticeable, although not enough to make a qualitative change over 5 BOs. In fact, as mentioned in the Introduction, the heating rate of a cloud of cold atoms inside a cavity has been measured in the experiment by Murch *et al* [31], and they found it to be consistent with the predictions of vacuum noise. The new feature in our problem is that the effective cavity drive detuning $\Delta_c^{\text{eff}}(t)$, which appears in the phase terms in Eq. (37), is Bloch periodic due to the meanfield dynamics.

The assumption of vacuum noise is often made in cavity optomechanics and allows some results to be derived analytically [30, 62–65]. The paradigmatic example of a cavity optomechanical system is a cavity with one end mirror attached to a spring or cantilever i.e. a harmonic oscillator driven by radiation pressure. Although ultra-cold atoms in a cavity can sometimes be mapped onto

this problem [28, 31, 41, 66, 67], that is not the case for the present system because the atomic Bloch states do not map very faithfully onto a single harmonic oscillator. Nonetheless, inspired by the optomechanical example we can tackle the problem by mapping it onto a collection of independent oscillators. The atomic excitation occupation $\delta N(t)$, which is plotted as the black (dashed) curves in Fig. 6, is then the sum over the occupation numbers of these independent oscillator modes $\delta N(t) = \sum_j \delta N_j(t)$. The details of this procedure will not be described here but are presented in the Appendix A. Suffice it to say that the basic idea is to consider the noise as a perturbation to the oscillator dynamics and then use Fermi's golden rule to develop a rate equation describing the occupation number dynamics of each oscillator [63]

$$\frac{d\langle\delta N_j\rangle}{dt} = (\Gamma_{uj} - \Gamma_{dj}) \langle\delta N_j\rangle + \Gamma_{uj}, \quad (38)$$

which is Eq. (A8) in Appendix A. In this expression Γ_{uj} and Γ_{dj} are the transition rates “up” and “down” for the j th oscillator and they are proportional to $S_{\mathcal{FF}}(-\omega_j)$ and $S_{\mathcal{FF}}(\omega_j)$, respectively, where $S_{\mathcal{FF}}(\omega)$ is the spectral density of force fluctuations (shot noise power spectrum). Thus, each oscillator is driven and damped by vacuum noise, with the rates of driving and damping being time dependent (due to the meanfield BO dynamics). Such a description allows an equilibrium to be reached and is the origin of the saturation effect visible in Fig. 7. Indeed, setting the left hand side of the rate equation to zero we obtain an expression for the equilibrium occupation of each oscillator

$$\langle\delta N_j\rangle_{\text{eq}}(t) = \frac{\Gamma_{uj}(t)}{\Gamma_{dj}(t) - \Gamma_{uj}(t)}. \quad (39)$$

By equilibrium here we mean a dynamic state in which δN_j is slaved to the instantaneous values of the transition rates. In the next two sections we examine the implications of the fluctuations for a precision measurement, i.e. how the fluctuations put a limit on how large a value of β can be chosen for a precision measurement.

VIII. SIGNAL-TO-NOISE RATIO: THEORY

We now explore how the inclusion of quantum noise affects the precision measurement proposal in [15]. Recall the basic idea shown schematically in Fig. 1: a cloud of cold atoms undergoes Bloch oscillations (e.g. due to gravity) inside a Fabry-Perot cavity, and the light field transmitted through the cavity is measured in order to determine the Bloch frequency. In order to quantify the measurement performance we will compute the signal-to-noise ratio using standard input-output theory [68].

Let us consider a double sided cavity with mirrors with matched reflectivities providing equal amplitude damping rates of $\kappa/2$. The quantum part of the input fields for both the top (driving side) and bottom (detection side)

mirrors is given by the electromagnetic vacuum. Since we are not going to consider classical fluctuations of the driving laser we do not include the meanfield part α of the input field, but introduce it via the hamiltonian in Eq. (3). In our consideration of system dynamics in earlier sections we implicitly assumed a single sided cavity giving an amplitude damping rate of κ , and associated with this decay is a Langevin noise term $\sqrt{2\kappa}\hat{\xi}(t)$. In a double sided cavity we have two *independent* noise terms of the form $\sqrt{\kappa}\{\hat{\xi}_t(t), \hat{\xi}_b(t)\}$. It can be shown that the dynamics of the intracavity system (both meanfield and fluctuations) are independent of whether we assume a double sided or single sided cavity as long as we divide the net damping equally among the two mirrors (provided they have matched reflectivities). The transmitted light field is the output field at the bottom mirror which is related to the input field at the bottom mirror as

$$\hat{a}_{\text{out}}(t) = -\hat{a}_{\text{in}}(t) + \sqrt{\kappa}\hat{a}(t) = -\hat{\xi}_b(t) + \sqrt{\kappa}\hat{a}(t) \quad (40)$$

where \hat{a}_{in} and \hat{a}_{out} in this equation refer to the fields at the bottom mirror. The transmitted photon current is given by the operator $\hat{I}_{\text{out}}(t) = \hat{a}_{\text{out}}^\dagger(t)\hat{a}_{\text{out}}(t)$, where again \hat{a}_{out} refers to the field leaving the bottom mirror.

An experimentally straightforward method for measuring the Bloch frequency consists of recording the transmitted photon current using a photodetector. It is useful to consider the Fourier transform of the data [69]

$$\hat{N}(\omega, T) = \int_0^T dt \cos(\omega t) \hat{I}_{\text{out}}(t) \quad (41)$$

and define the signal-to-noise ratio for the measurement as

$$\text{SNR} \equiv \frac{|\langle\hat{N}(\omega, T)\rangle|^2}{\Delta N^2(\omega, T)} \quad (42)$$

where $\Delta N^2(\omega, T) \equiv \langle(\hat{N} - \langle\hat{N}\rangle)^2\rangle$. Thus, the SNR is the ratio of the spectral density of the photon current to its variance and provides one measure of the sensitivity of the scheme.

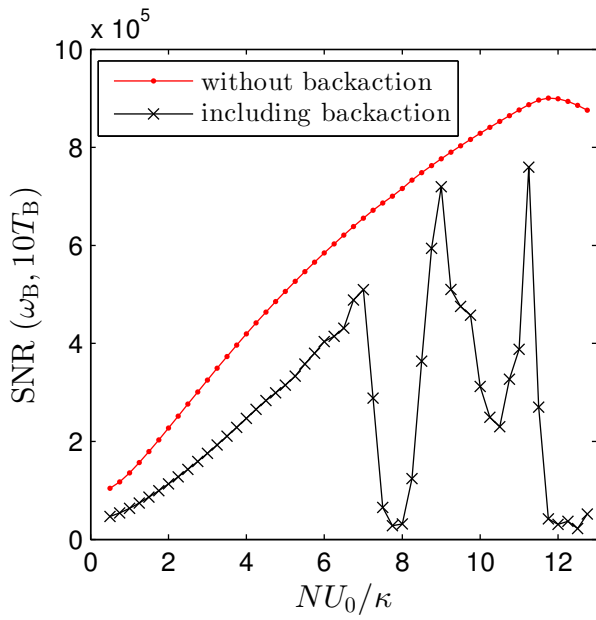
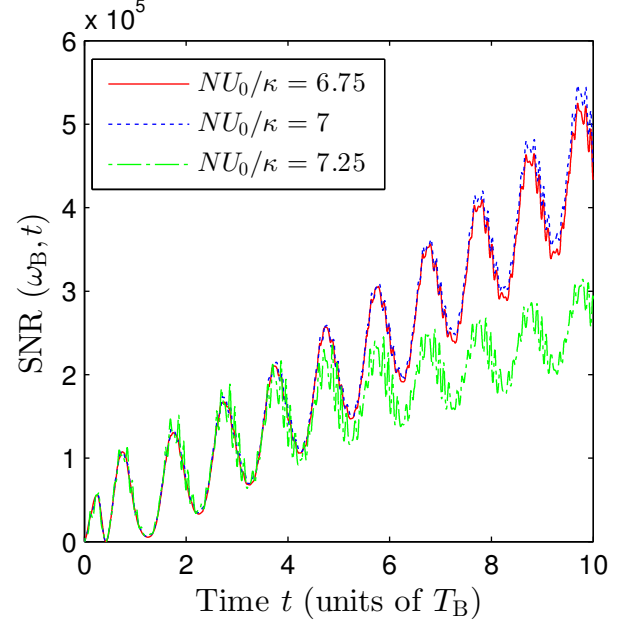
Let us first evaluate the SNR for a classical cavity field $\hat{a}(t) = \alpha(t)$. In this case one finds that the signal amplitude and variance are given by

$$\langle\hat{N}(\omega, T)\rangle = \kappa \int_0^T dt \cos(\omega t) |\alpha(t)|^2 \quad (43)$$

$$\Delta N^2(\omega, T) = \kappa \int_0^T dt \cos^2(\omega t) |\alpha(t)|^2. \quad (44)$$

In order to obtain an approximate magnitude for the SNR we further assume that the detection rate goes as $\approx R(1 + \epsilon \cos[\omega_B t])$ [15], where ϵ is the contrast parameter defined in Eq. (16). Setting the classical photon current $\kappa|\alpha(t)|^2$ in the above formulae equal to this detection rate gives

$$\text{SNR}(\omega_B, T) \approx \frac{\epsilon^2 R T}{2}. \quad (45)$$

(a) Signal-to-noise ratio as a function of $\beta = NU_0/\kappa$.

(b) Signal-to-noise ratio as a function of time

FIG. 8. (Color online) Plots of the SNR as a function of coupling strength β (a), and as a function of integration time for different values of β (b). In (a) the SNR was computed for an integration time of 10 Bloch periods (T_B) and the red (dots) curve gives the meanfield dynamics plus detector shot noise result, whilst the black (crosses) curve includes measurement backaction, i.e. the effect of quantum fluctuations upon the coupled atom-cavity dynamics. In (b) the red (solid) and blue (dotted) curves lie almost on top of each other and correspond to values of β just before the first dip in the SNR shown in Fig. 8a, whereas the green (dash-dotted) curve corresponds to a value of β in the dip. For all plots the minimum lattice depth was $3E_R$. Other parameters are the typical ones mentioned in the text.

Despite appearances, this result *does* include quantum noise to a certain degree because without the Langevin operators the variance given in Eq. (44) would have been zero, i.e. even when the cavity field is classical the output field contains a quantum part $\hat{a}_{\text{out}} = \alpha(t) - \hat{\xi}_b(t)$. Thus, the above calculation includes detector shot noise, also known as measurement imprecision [64], but neglects the effect of quantum fluctuations on the coupled dynamics inside the cavity, i.e. quantum measurement backaction. Note that this is a different approximation from the coherent state approximation used in Section VII, where quantum fluctuations were included in the cavity dynamics by using a Glauber coherent state, i.e. a state with vacuum noise, as cavity field, albeit one whose fluctuations are unaffected by the presence of the atoms.

The SNR given by Eq. (45) predicts that the sensitivity of the scheme can be increased indefinitely by increasing the mean total number of photons collected RT and also the contrast ϵ . The former effect is the standard one expected from the general theory of measurements with uncorrelated fluctuations. The latter is intuitively plausible too, but, however, can not be the whole truth because, as stated above, it neglects the effect of measurement backaction upon the dynamics which is expected to become important at larger values of β . When fluctuations are included $\hat{a}(t) = \alpha(t) + \delta\hat{a}(t)$, and the mean signal

amplitude is given by

$$\langle \hat{N}(\omega, T) \rangle = \kappa \int_0^T dt \cos(\omega t) (|\alpha(t)|^2 + \langle \delta\hat{a}^\dagger(t) \delta\hat{a}(t) \rangle). \quad (46)$$

In fact, this is not so very different from the meanfield photon number given by Eq. (43) because we are by design working in a regime where the meanfield dominates the fluctuations. However, the same is not true of the signal variance. The expression for the signal variance including fluctuations is cumbersome and is presented in Eq. (B1) in Appendix B. For present purposes it is enough to note that it includes a collection of terms that depend on integrals over two-time correlations of the photon fluctuations. These two-time correlations are challenging to evaluate numerically not only because the fluctuations occur on time scales κ^{-1} much shorter than the BOs, but also because they require the storage and manipulation of data at two times. Furthermore, the continuous driving by the BOs means that the correlations are not stationary in time, i.e. they do not just depend on $t_1 - t_2$, and this forces us to calculate the SNR in parallel to the system dynamics starting at $t = 0$. Unfortunately, due to limited computing power, we have only been able to track the SNR over ten Bloch periods which is certainly shorter than the coherence time of the BOs

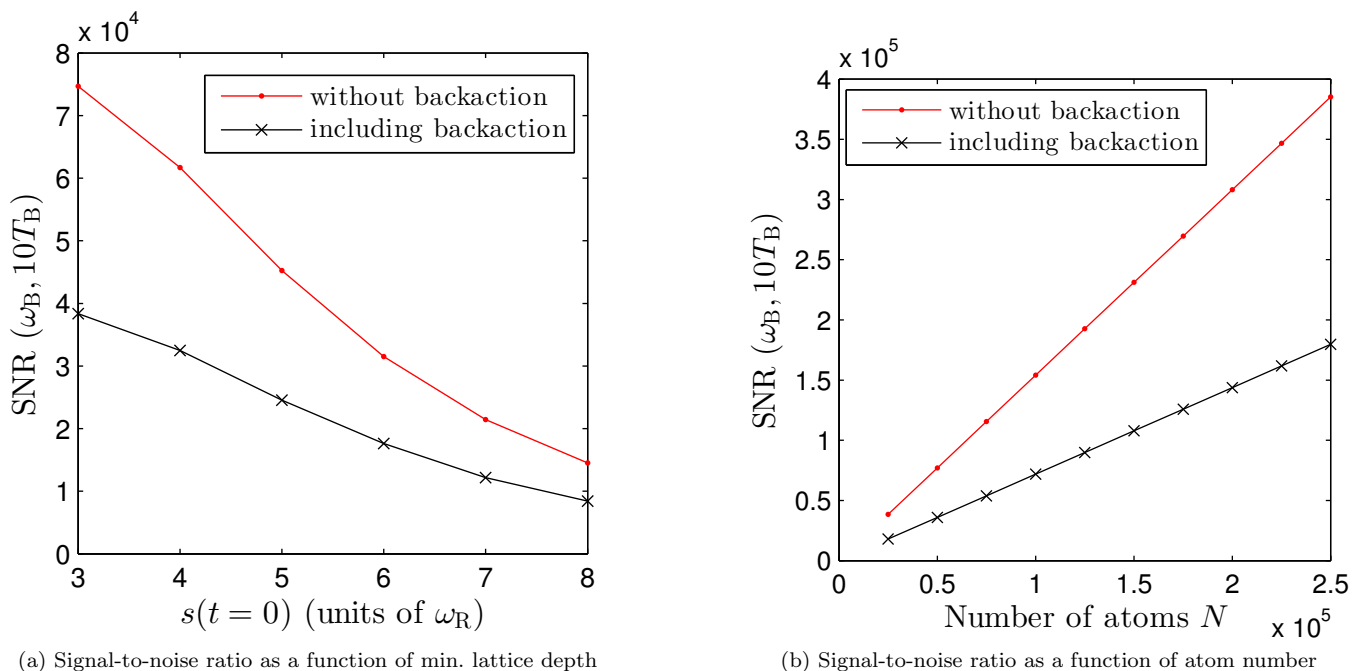


FIG. 9. (Color online) Plots of the SNR as a function of minimum lattice depth $s(t=0)$ (a), and as a function of atom number N (b). In both plots the red (dots) curves were computed from meanfield theory plus detector shot noise, and the black (crosses) curves were computed including quantum measurement backaction. For all points $NU_0/\kappa = 1$ and the signal is integrated over 10 Bloch periods. In (a) it is evident that the SNR decreases in both cases for larger lattice depths. In (b) it is evident that the SNR increases linearly as a function of N in both cases.

for the parameters we use. An actual experiment would, of course, not suffer from this limitation and would benefit from running until the BO coherence time is reached. The main steps of our algorithm for calculating the two time correlations are provided in Appendix B.

IX. SIGNAL-TO-NOISE RATIO: RESULTS

We now show how the SNR depends on the various system parameters. Due to the size of parameter space, this will not be an exhaustive study, but rather an *ad hoc* choice that nevertheless we hope is experimentally relevant. We begin by looking at the SNR as a function of the coupling parameter $\beta = NU_0/\kappa$. In Fig. 8a we plot the SNR evaluated at ω_B for an integration time of 10 Bloch periods. We change β by increasing U_0 but also change η to maintain the same minimum lattice depth of $3E_R$ throughout. The results without measurement backaction (i.e. the dynamics in the cavity is purely meanfield) are plotted by the red (dots) curve which monotonically increases until about $\beta = 12$. The initial increase of the SNR with β is in line with expectations based on Eq. (45). The turnover of the red curve near $\beta = 12$ is in a sense an artefact that arises from having evaluated our SNR at ω_B : it so turns out from the meanfield solution that for $\beta > 12$ the fraction of the power in the fundamental of $s(\omega)$ begins to decline and is diverted to higher harmonics. However, there is no real reason other than simplicity

to only consider $\text{SNR}(\omega_B)$ (any harmonic of ω_B gives information about the applied force and inclusion of all of them in the data analysis would extract the maximum possible information from the measurement). The full calculation including measurement backaction is plotted by the black (crosses) curve. The first thing to notice is that measurement backaction always lowers the SNR. Secondly, the full SNR monotonically increases only until $\beta \approx 7$, and thereafter suffers from dramatic dips which we explain below as being due to resonances with quasi-particle excitation energies. These two observations are the main results of this paper. In Fig. 8b we plot the SNR as function of the total integration time for three values of β , two before the first dip in the SNR and one in it. This plot further illustrates that for $\beta > 7$ there is a dramatic lowering of the SNR. The BO dynamics are also clearly visible due to the fact that the contrast is periodically growing and shrinking as the lattice depth grows and shrinks.

integration time of $10T_B$. Whereas for the value (green solid line) to the right of the peak one can see that the SNR has more or less flat lined near $t \approx 10T_B$. Thus in Fig. 8a (with integration time of $10T_B$), for points to the left of the peak, the SNR is still gaining due to the increased measurement strength whereas this is not the case to the right of the peak.

In Figs. 9a and 9b we show how the SNR depends on other parameters, namely the lattice depth and total number of atoms. In particular, in Fig. 9a we plot the

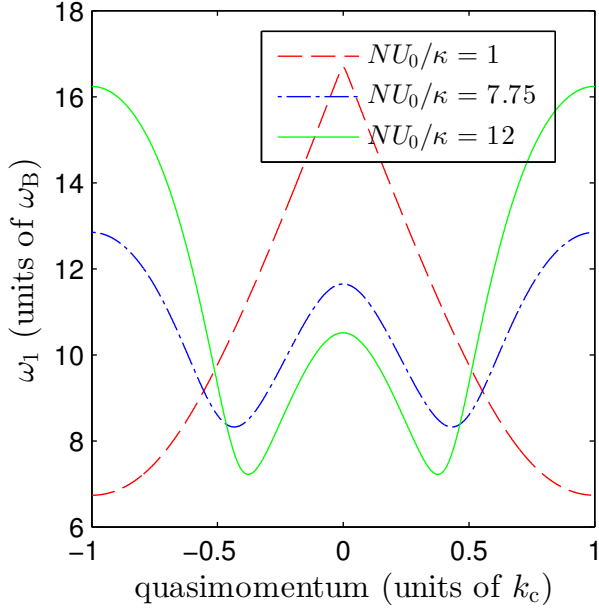
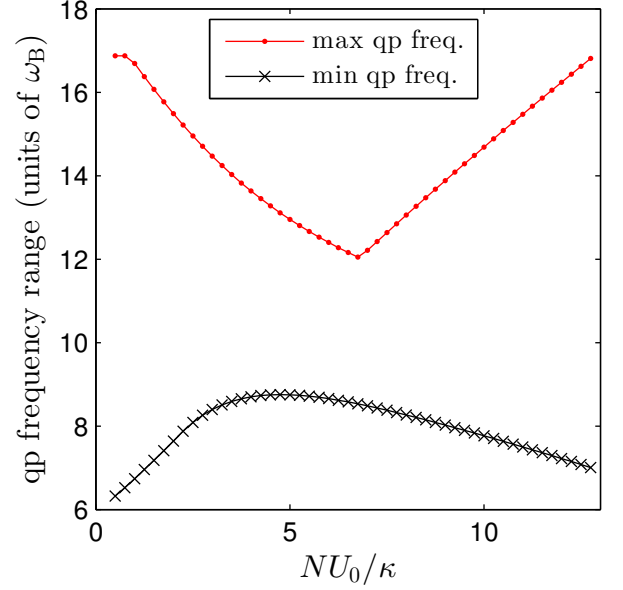
(a) Lowest excitation frequency for three different values of β (b) Lowest excitation frequency for all q as a function of β

FIG. 10. (Color online) Plots of the lowest quasiparticle excitation frequency ω_1 about the adiabatic solution. In (a) this is given as a function of quasimomentum for three different values of β : For small β (red dashed curve) the minimum of the frequency occurs at $q = \pm 1$, but for larger values of β the minimum shifts in to smaller values of q . Since each quasiparticle excitation has an energy varying with q , in (b) we plot the range of possible excitation frequencies contained in ω_1 for all q as a function of β . The frequency units are the Bloch frequency ω_B .

SNR as a function of the minimum lattice depth in the cavity for the coupling value $NU_0/\kappa = 1$. The lattice depth is changed by increasing η . The red (dots) curve gives the SNR calculated using only meanfield dynamics plus the effect of shot noise at the detector and justifies the claim made in Section IV that for larger lattice depth the contrast decreases. The SNR calculation including measurement backaction fluctuations is given by the black (crosses) curve, and has the same qualitative behaviour but is somewhat lower. Fig. 9b plots the SNR as a function of N , where for different values of N we keep $NU_0/\kappa = 1$ constant by scaling U_0 . We also scale the pump strength η to maintain the same intracavity lattice depth $s(t)$ in all the cases. As we pointed out in Section IV, this method of scaling the system variables leaves the form of the meanfield and fluctuation equations unchanged. The only quantitative change is that the meanfield cavity field solution $\alpha(t)$ is scaled by the same \sqrt{r} factor as the pumping. This leads to a linear scaling of the SNR as a function of N (with and without fluctuations) as shown in the plot. It is interesting to note that the rate of increase is different for the calculation including fluctuations compared to that without. Clearly there is a gain in the SNR with N , but one has to also keep in mind that in our treatment we have completely ignored the atom-atom collisional interaction which will eventually become important at high atom densities.

Finally, we shall explain the physical origin of the complicated series of dips in the SNR when $\beta > 7$ that are

seen in Fig. 8a. Consider the spectrum of quasiparticle excitations about the adiabatic meanfield solution introduced in Section VI. For the example shown in Fig. 5a, the smallest excitation frequency occurs at the band edge $q = \pm 1$ and the largest at $q = 0$. As β is increased in the usual manner (holding the minimum lattice depth constant), the q -dependence of the quasiparticle spectrum evolves, as shown for the quasiparticle mode ω_1 in Fig. 10a. Thus, the range of frequencies (i.e. across the entire Brillouin zone) contained in ω_1 also evolves with β and is shown in Fig. 10b. If the meanfield dynamics happens to contain any frequencies that fall in this range there is clearly the possibility of a resonance, exciting quasiparticles and lowering the SNR. This is exactly what happens as can be seen from Fig. 11 which plots the total power in the harmonics of ω_B that fall in the frequency range covered by ω_1 . The two peaks in Fig. 11 at $\beta \approx 8$ and $\beta \approx 12$ coincide exactly with the dips in Fig. 8a. Referring back to the inset in Fig. 3b, which was deliberately evaluated at $\beta = 7.75$ for this very purpose, we can see the part of the meanfield spectrum that falls in the range spanned by ω_1 . In the absence of BOs the quasiparticle excitation ω_1 is very narrow, with a width given by the imaginary part γ_1 evaluated at $q = 0$. However, the BO dynamics effectively broadens the resonance by orders of magnitude to that shown in Fig. 10b and this has a dramatic effect on the SNR.

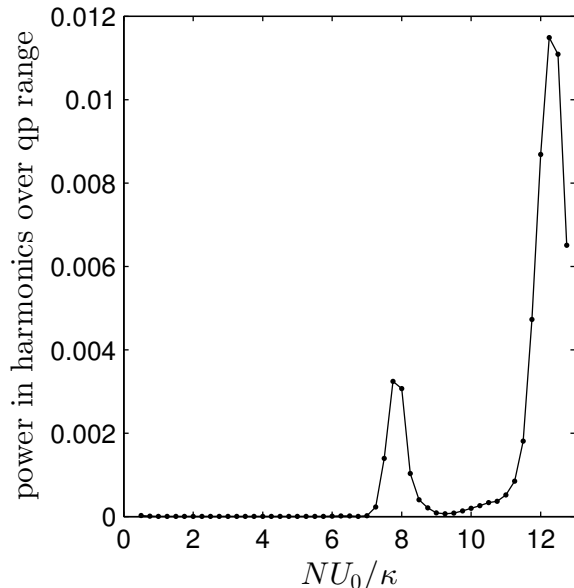


FIG. 11. The normalized power in the harmonics of ω_B as calculated from the Fourier transform of the meanfield solution (see Fig. 3b) that lies in the frequency range of the lowest quasiparticle excitation (see Fig. 10b).

X. SUMMARY AND CONCLUSIONS

In this paper we have extended our previous analysis of Bloch oscillations of ultracold atoms inside a cavity to include the effects of quantum noise in the electromagnetic field. The quantum noise originates from the open nature of the cavity and can be interpreted as a form of quantum measurement backaction because it perturbs the dynamics. The magnitude of the backaction is controlled by the dimensionless atom-light coupling parameter $\beta = NU_0/\kappa$ and we find that it can strongly affect the sensitivity of a measurement of the Bloch oscillation frequency ω_B and therefore the determination of the magnitude of the external force F driving them.

Our treatment is based upon the coupled Heisenberg equations of motion for the atoms and light which we linearize about their meanfield solutions, i.e. a Bogoliubov level approximation. We solve the meanfield level dynamics exactly and hence coherent effects such as Landau-Zener tunneling between bands are fully taken into account. A spectral decomposition of the meanfield solution shows that it is dominated by ω_B and its first few harmonics, but as β is increased spectral power begins to spread to higher frequencies.

Quantum noise is introduced via Langevin operators which act as inhomogeneous source terms in the Heisenberg equations. These terms lead to both the creation and annihilation of quasiparticles (quantized excitations with a mixed atom-light character) and hence can both heat and cool the system. If the system is started off with no quasiparticles, i.e. at zero temperature, the number of

excitations initially grows in time at a rate that increases with β . However, the number of excitations eventually saturates due to competition between the cooling and heating processes (provided we are in the cooling regime $\Delta_c^{\text{eff}} = \Delta_c - NU_0\langle\cos^2(x)\rangle < 0$) with the “equilibrium” number of excitations being dynamic in the sense that it is modulated by the Bloch oscillation.

In order to gain some insight into the numerical calculations we used Fermi’s golden rule to develop a semi-analytic model for the heating rate in terms of a simple rate equation for the number of atomic excitations. In so doing we approximated the cavity light field by a coherent state whose quantum fluctuations are the same as those of the vacuum. This is a common approximation in cavity optomechanics but ignores the quantum correlations that build up between the atoms and the light. Comparing this with the exact numerical results for the number of atomic excitations, we infer that the field is close to a coherent state for small β , but differs from it as β is increased, as expected.

The above calculations can be applied to the estimation of the signal-to-noise ratio for a continuous measurement of ω_B . For example, we find that the SNR decreases with intracavity lattice depth, and increases with the number of atoms. Our principal result, however, concerns the dependence upon β . We find that the SNR can be severely reduced due to resonances between the quasiparticle spectrum and the Bloch oscillating meanfield for certain ranges of β . Indeed, the SNR behaviour depicted in Fig. 8 is much more complicated than that found in the standard example of a quantum limited position measurement of a harmonic oscillator, e.g. the end mirror of a resonant cavity [64]. In that system, the SNR is determined by the competition between the “measurement imprecision” (detector shot noise), which decreases with increasing measurement strength, and the measurement backaction, which increases with increasing measurement strength, and correlations between the two can be ignored to a good approximation. This leads to a smooth curve (see Fig. 5 on p.1171 of the review [64]) with a single maximum at the measurement strength where the two effects are equal. This is where the measurement should be performed for maximum sensitivity. By contrast, in our case we have a cloud of atoms occupying Bloch states in an optical lattice and thus our system does not correspond very well to a single harmonic oscillator (except in the limit where the lattice is extremely weak so that the atoms are predominantly in a state which is uniform in space [28], but then Landau-Zener tunneling will be so severe that the atoms will quickly fall out of the lattice when the external force F is applied). Add to this the fact that our system is driven by an external force and so scans through the entire Bloch band in a time-dependent fashion, leading to the possibility of resonances, and it is not surprising that our resulting SNR in Fig. 8a does not have a simple maximum as a function of β . However, we can make the parameter dependent statement that it seems safest to choose $\beta < 7$ which lies below the point

where the resonances set in (and for $\beta > 25$ we find optical bistability which will destroy the Bloch oscillations [32]). The resonances only occur in the calculation when quantum measurement backaction is included and so provide a salutary example of when the latter is important. Nevertheless, away from the resonances the SNR for this continuous measurement is large and is in pretty good agreement with an approximate calculation based upon purely meanfield dynamics in the cavity plus detector shot noise.

In comparison to previously studied cold atom cavity-QED systems, or even cavity optomechanical systems, a new feature of our Bloch oscillating system is the time-dependence of the meanfield. Apart from the resonances discussed above, this also has implications for the computational scheme we use to calculate the results. For example, all the fluctuation modes should be orthogonal to the meanfield mode as well as to each other, and hence they also evolve with time. Furthermore, the two-time correlation functions that are needed to calculate the signal variance that enters the SNR are not stationary in time, meaning that a large amount of data must be stored. This is especially true because the Bloch period is roughly three orders of magnitude larger than the quantum fluctuation timescale $1/\kappa$ and hence the calculation of the SNR over even a few Bloch periods is quite intensive in the regime where the coherent state approximation breaks down. In non-cavity BO experiments it has been shown that coherent dynamics can run for thousands of Bloch periods [9]. In a continuous measurement scheme, such as that proposed here, the quantum measurement backaction reduces the coherence time but unfortunately we have been unable to go much beyond ten Bloch periods with our numerical computations of the SNR and thereby find this coherence time for our scheme (we have, however, given an estimate in [15] based upon the idea that the spontaneous emission rate

sets the upper limit on coherent dynamics). Nonetheless, our short time calculations illustrate quantitatively that it may be advantageous to remain at small β and integrate for longer times. In future work we hope to develop approximations and/or better numerical methods to treat large values of the coupling.

frequency and the minimum of the atomic fluctuation spectrum leads to enhanced occupation of the fluctuation modes.

XI. ACKNOWLEDGEMENTS

This research was funded by the Natural Sciences and Engineering Research Council of Canada. We thank A. Blais, E. A. Hinds, J. Goldwin, J. Larson, and M. Trupke for discussions related to this work and D. Nagy for helpful correspondence.

Appendix A: Coherent State Approximation

In this appendix we provide details of how the coherent state approximation described in VII can be used to derive a simple approximation for the atomic fluctuation dynamics. Consider Eq. (24b) for the atomic fluctuation dynamics, and let us decompose the atomic fluctuation operator (working in the TF) into the instantaneous eigenbasis $|\nu_k(t)\rangle$ of the time-dependent meanfield hamiltonian $\bar{\mathcal{H}}(t)$

$$\delta\hat{\Psi}_\perp(t) = \sum_k |\nu_k(t)\rangle \delta\hat{b}_k(t) \quad (\text{A1})$$

$$\bar{\mathcal{H}}(t)|\nu_k(t)\rangle = E_k(t)|\nu_k(t)\rangle \quad (\text{A2})$$

where we have dropped the coordinate dependence of the atomic fluctuation operator and we use bra-ket notation for the single particle states. On substituting the decomposition Eq. (A1) into Eq. (24b) we obtain

$$\begin{aligned} \frac{d\delta\hat{b}_j(t)}{dt} = & -iE_j(t)\delta\hat{b}_j(t) - \sum_k \langle\nu_j(t)| \frac{d}{dt} |\nu_k(t)\rangle \delta\hat{b}_k(t) \\ & - i\sqrt{N}U_0 (\alpha^*(t)\delta\hat{a}(t) + \alpha(t)\delta\hat{a}^\dagger(t)) \langle\nu_j(t)| \hat{P}(t) \cos^2(x) |\bar{\varphi}(t)\rangle. \end{aligned} \quad (\text{A3})$$

Clearly in the above form the dynamics of the $\delta\hat{b}_j(t)$ are coupled amongst themselves. To decouple the dynamics consider the second term (with the time derivative) on the right hand side of Eq. (A3). It can be shown that ([70]):

$$\langle\nu_j(t)| \frac{d}{dt} |\nu_k(t)\rangle \stackrel{j \neq k}{=} \frac{1}{E_k(t) - E_j(t)} \langle\nu_j(t)| \frac{d\bar{\mathcal{H}}(t)}{dt} |\nu_k(t)\rangle$$

Now for $k = j \pm 1$, the matrix element goes to zero for symmetry reasons and for other k , the energy difference

will make the term smaller. Thus we need to only take care of the term for $k = j$. Focusing on that now we have

$$\frac{d}{dt} (\langle\nu_k(t)|\nu_k(t)\rangle) = \langle\nu_k(t)| \frac{d}{dt} |\nu_k(t)\rangle + h.c. = 0$$

i.e. the derivative term with $j = k$ is purely imaginary. For the time dependent hamiltonian $\bar{\mathcal{H}}(t)$ the potential term $\cos^2(x)$ has an inversion symmetry about $x = 0$ and we can always choose the instantaneous eigenbasis $|\nu_k(t)\rangle$ to have real coefficients when expanded over plane

waves. As a result the above term goes to zero and the time derivative terms can be excluded. From Eq. (36) we can see that the last term in Eq. (A3), which depends on the light field fluctuation, can couple the different modes $\delta\hat{b}_j(t)$. At this juncture the coherent state approximation is made which assumes the light field fluctuations are independent of the atomic fluctuations i.e.

$$\delta\hat{a}(t) \approx \hat{d}(t) \equiv \sqrt{2\kappa} \int_0^t d\tau e^{-iA(t)(t-\tau)} \hat{\xi}(\tau). \quad (\text{A4})$$

This ensures that the different modes are uncoupled and we can write down their independent dynamics as

$$\frac{d\delta\hat{b}_j}{dt} = -iE_j\delta\hat{b}_j(t) - u_j(t)\hat{\mathcal{F}}(t) \quad (\text{A5})$$

where

$$u_j(t) = i\sqrt{N}U_0\langle\nu_j(t)|\hat{P}(t)\cos^2(x)|\bar{\varphi}(t)\rangle \quad (\text{A6})$$

$$\hat{\mathcal{F}}(t) = \left(\alpha^*(t)\hat{d}(t) + \alpha(t)\hat{d}^\dagger(t)\right). \quad (\text{A7})$$

These equations describe the atomic fluctuation dynamics in terms of a collection of *independent* oscillator modes that are acted upon by the shot noise force $\hat{\mathcal{F}}(t)$. As described in [63], we can now use Fermi's golden rule to derive a rate equation for each of the oscillator occupation numbers $\delta N_j(t) = \langle\delta\hat{b}_j^\dagger\delta\hat{b}_j\rangle$

$$\frac{d\langle\delta N_j\rangle}{dt} = (\Gamma_{uj} - \Gamma_{dj}) \langle\delta N_j\rangle + \Gamma_{uj} \quad (\text{A8})$$

where the damping and diffusion rates are

$$\Gamma_{uj} = |u_j|^2 S_{\mathcal{FF}}(-\omega_j); \quad \Gamma_{dj} = |u_j|^2 S_{\mathcal{FF}}(\omega_j).$$

These depend on the spectral density (power spectrum) of the shot noise force

$$S_{\mathcal{FF}}(\omega) = \frac{2\kappa\bar{n}}{(\Delta_c^{\text{eff}} + \omega)^2 + \kappa^2}. \quad (\text{A9})$$

In the above expressions the shot noise spectrum is evaluated at the shifted oscillator frequencies defined by $\omega_j = E_j(t) - \mu(t)$ with the instantaneous chemical potential $\mu(t) = \langle\bar{\varphi}(t)|\hat{\mathcal{H}}(t)|\bar{\varphi}(t)\rangle$. This shifting helps in removing the slow time dependence of the couplings u_j (derived from the meanfield Bloch oscillations) when developing the rate equations. Since the total number of atomic excitations $\delta N(t) = \sum_j \delta N_j(t)$, Eq. (A8) gives an approximate description of the atomic fluctuation occupation number. Since the damping and diffusion rates for the different oscillators are not the same, it is in general not possible to write down an equation similar in form to Eq. (A8) for $\delta N(t)$.

As mentioned in the main part of the paper in Section VII, the system can reach a dynamic steady state in the sense that δN_j is slaved to the instantaneous values of the transition rates. In this case, we can put $d\langle\delta N_j\rangle/dt = 0$ and thus

$$\langle\delta N_j\rangle_{\text{eq}}(t) = \frac{\Gamma_{uj}(t)}{\Gamma_{dj}(t) - \Gamma_{uj}(t)} = -\frac{(\Delta_c^{\text{eff}}(t) + \omega_j)^2 + \kappa^2}{4\Delta_c^{\text{eff}}(t)\omega_j(t)} \quad (\text{A10})$$

where the negative sign is fine because $\Delta_c^{\text{eff}}(t)$ is negative on the cooling side of the effective resonance.

Appendix B: Two time correlation calculation

When the intracavity light field is written as $\hat{a}(t) = \alpha(t) + \delta\hat{a}(t)$, the signal variance is given by:

$$\begin{aligned} \langle\Delta\hat{N}^2(\omega, T)\rangle &= \kappa \left[\int_0^T \cos^2(\omega t) (|\alpha(t)|^2 + \langle\delta\hat{a}^\dagger\delta\hat{a}(t)\rangle) dt \right] + 2\kappa^2 \text{Re} \left[\int_0^T dt_1 dt_2 \cos(\omega t_1) \cos(\omega t_2) \alpha(t_1) \alpha(t_2) \langle\delta\hat{a}^\dagger(t_1) \delta\hat{a}^\dagger(t_2)\rangle \right] \\ &+ \kappa^2 \left[\int_0^T dt_1 dt_2 \cos(\omega t_1) \cos(\omega t_2) \alpha^*(t_1) \alpha(t_2) \langle\delta\hat{a}(t_1) \delta\hat{a}^\dagger(t_2)\rangle + \int_0^T dt_1 dt_2 \alpha(t_1) \alpha^*(t_2) \cos(\omega t_1) \cos(\omega t_2) \langle\delta\hat{a}^\dagger(t_1) \delta\hat{a}(t_2)\rangle \right] \\ &- 2(\kappa)^{3/2} \text{Re} \left[\int_0^T dt_1 dt_2 \alpha^*(t_1) \alpha(t_2) \cos(\omega t_1) \cos(\omega t_2) \langle\hat{\xi}_b(t_1) \delta\hat{a}^\dagger(t_2)\rangle \theta(t_2 - t_1) \right]. \end{aligned} \quad (\text{B1})$$

In this appendix we provide details of how we numerically compute the signal variance (and hence the SNR). The important extra computational step compared to the covariance matrix calculation in Eq. (31) is the evaluation of the two time correlations such as $\langle\delta\hat{a}^\dagger(t_1) \delta\hat{a}^\dagger(t_2)\rangle$. In the vector notation for the fluctuations, the two time correlations are elements of the correlation matrix

$\mathbf{\Lambda}(t_1, t_2) = \langle\hat{R}(t_1) \hat{R}^T(t_2)\rangle$. The time evolution for the correlation matrix is given by:

$$i \frac{d}{dt} \mathbf{\Lambda}(t, t_0) = \mathbf{M}(t) \mathbf{\Lambda}(t, t_0) + i \langle\hat{Z}(t) \hat{R}^T(t_0)\rangle. \quad (\text{B2})$$

Let us consider the case when $t > t_0$. Then the last term in above equation gives a correlation between the

Langevin operators at some future time t and the system fluctuation operators at t_0 . Due to the delta-correlated nature of the Langevin noise this term will be zero. This means that Eq. (B2) becomes homogeneous and we can solve it with the initial condition at $t = t_0$, $\mathbf{\Lambda}(t_0, t_0) = \mathbf{C}(t_0)$. Also note that the time evolution operator for the numerical evolution in Eq. (B2) is same as the one for the covariance matrix [denoted by $\mathbf{G}(t)$ in Eq. (31)], which is an expression of the quantum regression theorem [68]. A separate computation for $t < t_0$ is not needed since they are related to the elements of $\mathbf{\Lambda}(t, t_0)$ with $t > t_0$ by complex conjugation. For example:

$$\langle \delta \hat{a}^\dagger(t_0) \delta \hat{a}(t) \rangle = \langle \delta \hat{a}(t) \delta \hat{a}^\dagger(t_0) \rangle^*.$$

We can evaluate the correlation $\langle \hat{\xi}_b(t_1) \delta \hat{a}^\dagger(t_2) \rangle$ using a similar approach as above for the time evolution of the vector $\langle \hat{\xi}_b(t_1) \hat{R}(t_2) \rangle$. In this case the initial condition for the evolution is $\langle \hat{\xi}_b(t_0) \delta \hat{a}^\dagger(t_0) \rangle = \sqrt{\kappa}/2$. Since the evolution operators for the correlation matrix and covariance matrix evolution are the same the calculation can be performed without additional computational cost. The main

difficulty in computing the signal variance arises from the fact that the two time correlation functions are not stationary. As a result, in order to evaluate the integrals in Eq. (B1) the correlation matrix needs to be computed for all values of $0 < t_1, t_2 < T$. This is the memory intensive step in the computation and we simplify the situation by performing the correlation matrix computation over a coarser grid than the one used in the numerical solution of Eq. (31). This is justified since we find typically the correlation matrix elements do not change significantly over the very short time steps chosen in the solution of Eq. (31). Moreover, for the results presented in Section VIII, we have taken care to check that the numerical solutions converge to a value independent of the size of the coarse grid. The necessity of evaluating two-time correlators over a two dimensional time grid is the main limiting factor to the maximum integration time for the SNR calculations. Another difficulty that we faced was that for β values larger than the ones that we have presented here we found that the size of the coarse grid needs to be essentially matched with the size of the finer computational grid over which Eq. (31) is solved. As a result the calculation becomes very memory intensive indeed.

-
- [1] F. Bloch, Z. Phys. **52**, 555 (1928); C. Zener, Proc. R. Soc. London, Ser. A **145**, 523 (1934).
 - [2] M. Ben Dahan, E. Peik, J. Reichel, Y. Castin, and C. Salomon, Phys. Rev. Lett. **76**, 4508 (1996); E. Peik, M. Ben Dahan, I. Bouchoule, Y. Castin, and C. Salomon, Phys. Rev. A **55**, 2989 (1997).
 - [3] S. R. Wilkinson, C. F. Bharucha, K. W. Madison, Q. Niu, and M. G. Raizen, Phys. Rev. Lett. **76**, 4512 (1996).
 - [4] R. Battesti, P. Cladé, S. Guellati-Khélifa, C. Schwob, B. Grémaud, F. Nez, L. Julien, and F. Biraben, Phys. Rev. Lett. **92**, 253001 (2004); P. Cladé, E. de Mirandes, M. Cadoret, S. Guellati-Khélifa, C. Schwob, F. Nez, L. Julien, and F. Biraben, *ibid.* **96**, 033001 (2006).
 - [5] I. Carusotto, L. Pitaevskii, S. Stringari, G. Modugno, and M. Inguscio, Phys. Rev. Lett. **95**, 093202 (2005).
 - [6] B.P. Anderson and M.A. Kasevich, Science **282**, 1686 (1998).
 - [7] O. Morsch, J. H. Müller, M. Cristiani, D. Ciampini, and E. Arimondo, Phys. Rev. Lett. **87**, 140402 (2001).
 - [8] G. Roati, E. de Mirandes, F. Ferlaino, H. Ott, G. Modugno, and M. Inguscio, Phys. Rev. Lett. **92**, 230402 (2004).
 - [9] G. Ferrari, N. Poli, F. Sorrentino, and G. M. Tino, Phys. Rev. Lett. **97**, 060402 (2006).
 - [10] S. Burger, F. S. Cataliotti, C. Fort, F. Minardi, M. Inguscio, M. L. Chiofalo and M. P. Tosi, Phys. Rev. Lett. **86**, 4447 (2001).
 - [11] B. Wu and Q. Niu, N. J. Phys. **5**, 104 (2003).
 - [12] V. V. Ivanov, A. Alberti, M. Schioppo, G. Ferrari, M. Artoni, M. L. Chiofalo, and G. M. Tino, Phys. Rev. Lett. **100**, 043602 (2008).
 - [13] N. Poli, F.-Y. Wang, M. G. Tarallo, A. Alberti, M. Prevedelli, and G. M. Tino, Phys. Rev. Lett. **106**, 038501 (2011).
 - [14] M.G. Tarallo, A. Alberti, M.L. Chiofalo, F.-Y. Wang, and G. M. Tino, arXiv:1207.2123v1
 - [15] B. Prasanna Venkatesh, M. Trupke, E. A. Hinds and D. H. J. O'Dell, Phys. Rev. A **80**, 063834 (2009).
 - [16] B. M. Peden, D. Meiser, M. L. Chiofalo, and M. J. Holland, Phys. Rev. A **80**, 043803 (2009).
 - [17] A. Boca, R. Miller, K. M. Birnbaum, A. D. Boozer, J. McKeever, and H.J. Kimble, Phys. Rev. Lett. **93** 233603 (2004).
 - [18] P. Maunz, T. Puppe, I. Schuster, N. Syassen, P. W. H. Pinkse, and G. Rempe, Phys. Rev. Lett. **94** 033002 (2005).
 - [19] J. Klinner, M. Lindholdt, B. Nagorny, and A. Hemmerich Phys. Rev. Lett. **96**, 023002 (2006)
 - [20] Y. Colombe, T. Steinmetz, G. Dubois, F. Linke, D. Hunger, and J. Reichel, Nature (London) **450**, 272 (2007).
 - [21] H. Mabuchi, Q. A. Turchette, M. S. Chapman, and H. J. Kimble, Opt. Lett. **21**, 1393 (1996); C. J. Hood, M. S. Chapman, T. W. Lynn, and H. J. Kimble, Phys. Rev. Lett. **80**, 4157 (1998).
 - [22] P. Münstermann, T. Fischer, P. W. H. Pinkse, and G. Rempe, Opt. Commun. **159**, 63 (1999); P. Münstermann, T. Fischer, P. Maunz, P. W. H. Pinkse, and G. Rempe, Phys. Rev. Lett. **82**, 3791 (1999).
 - [23] M. Trupke, J. Goldwin, B. Darquié, G. Dutier, S. Eriksen, J. Ashmore, and E. A. Hinds, Phys. Rev. Lett. **99**, 063601 (2007).
 - [24] J. Ye, D. W. Vernooy, and H. J. Kimble, Phys. Rev. Lett. **83**, 4987 (1999); C. J. Hood, T. W. Lynn, A. C. Doherty, A. S. Parkins, and H. J. Kimble, Science **287**, 1447 (2000).
 - [25] P. W. H. Pinkse, T. Fischer, P. Maunz, and G. Rempe, Nature (London) **404**, 365 (2000).

- [26] B. Nagorny, Th. Elsässer, and A. Hemmerich Phys. Rev. Lett. **91**, 153003 (2003)
- [27] S. Gupta, K. L. Moore, K. W. Murch, and D. M. Stamper-Kurn, Phys. Rev. Lett. **99**, 213601 (2007).
- [28] F. Brennecke, S. Ritter, T. Donner, and T. Esslinger, Science **322**, 235 (2008); S. Ritter, F. Brennecke, K. Baumann, T. Donner, C. Guerlin and T. Esslinger, App. Phys. B **95**, 213 (2009).
- [29] P. Horak, G. Hechenblaikner, K. M. Gheri, H. Stecher, and H. Ritsch, Phys. Rev. Lett. **79**, 4974 (1997); P. Domokos and H. Ritsch, Phys. Rev. Lett. **89**, 253003 (2002).
- [30] F. Marquardt, J. P. Chen, A. A. Clerk, and S. M. Girvin, Phys. Rev. Lett. **99**, 093902 (2007).
- [31] K. W. Murch, K. L. Moore, S. Gupta, and D. M. Stamper-Kurn, Nature Physics **4**, 561 (2008); N. Brahms, T. Botter, S. Schreppler, D. W. C. Brooks, and D. M. Stamper-Kurn, Phys. Rev. Lett. **108**, 133601 (2012).
- [32] B. Prasanna Venkatesh, J. Larson, and D. H. J. O'Dell, Phys. Rev. A **83**, 063606 (2011).
- [33] W. Chen, D. S. Goldbaum, M. Bhattacharya and P. Meystre, Phys. Rev. A **81**, 053833 (2010).
- [34] M. Coles and D. Pelinovsky, Studies in Applied Mathematics **128**, 300 (2012).
- [35] B. Wu and Q. Niu, Phys. Rev. A **64**, 061603(R) (2001); B. Wu, R. B. Diener, and Q. Niu, *ibid.* **65**, 025601 (2002); B. Wu and Q. Niu, New J. Phys. **5**, 104 (2003).
- [36] D. Diakonov, L. M. Jensen, C. J. Pethick, and H. Smith, Phys. Rev. A **66**, 013604 (2002); M. Machholm, C. J. Pethick, and H. Smith, *ibid.* **67**, 053613 (2003); M. Machholm, A. Nicolin, C. J. Pethick, and H. Smith, *ibid.* **69**, 043604 (2004).
- [37] E. J. Mueller, Phys. Rev. A **66**, 063603 (2002).
- [38] A. Smerzi, A. Trombettoni, P. G. Kevrekidis, and A. R. Bishop, Phys. Rev. Lett. **89**, 170402 (2002).
- [39] P. Horak and H. Ritsch, Phys. Rev. A **63**, 023603 (2001).
- [40] G. Szirmai, D. Nagy, and P. Domokos, Phys. Rev. Lett. **102**, 080401 (2009).
- [41] G. Szirmai, D. Nagy, and P. Domokos, Phys. Rev. A **81**, 043639 (2010).
- [42] S. K. Steinke and P. Meystre, Phys. Rev. A **84**, 023834 (2011).
- [43] C. Maschler and H. Ritsch, Phys. Rev. Lett. **95**, 260401 (2005); I. B. Mekhov, C. Maschler and H. Ritsch, Nat. Phys. **3**, 319 (2007); C. Maschler, I. B. Mekhov, and H. Ritsch, Euro. Phys. J. D **46**, 545 (2008).
- [44] J. Larson, B. Damski, G. Morigi, and M. Lewenstein, Phys. Rev. Lett. **100**, 050401 (2008); J. Larson, S. Fernandez-Vidal, G. Morigi, and M. Lewenstein, New J. Phys **10**, 045002 (2008).
- [45] R. Mottl *et al.*, Science **336**, 1570 (2012).
- [46] M. Gustavsson, E. Haller, M. J. Mark, J. G. Danzl, G. Rojas-Kopeinig, and H.-C. Nägerl, Phys. Rev. Lett. **100**, 080404 (2008).
- [47] F.W.J. Olver *et al.* (Eds), *NIST Handbook of Mathematical Functions* (C.U.P., Cambridge, 2010).
- [48] M. Glück, A. R. Kolovsky, H. J. Korsch, Phys. Rep. **366**, 103 (2002).
- [49] W. V. Houston, Phys. Rev. **57**, 184 (1940).
- [50] H. Kroemer, Am. J. Phys. **54**, 177 (1986).
- [51] B. Wu and Q. Niu, Phys. Rev. A **61**, 023402 (2000).
- [52] C. J. Pethick and H. Smith, *Bose Einstein Condensation in Dilute Gases*, 2nd ed. (Cambridge University Press, Cambridge, 2008).
- [53] L. P. Pitaevskii and S. Stringari, *Bose-Einstein Condensation* (Oxford University Press, New York, 2003).
- [54] M. Lewenstein and L. You, Phys. Rev. Lett. **77**, 3489 (1996).
- [55] Y. Castin and R. Dum, Phys. Rev. Lett. **79**, 3553 (1997); Y. Castin and R. Dum, Phys. Rev. A **57**, 3008 (1998).
- [56] S. A. Gardiner, D. Jaksch, R. Dum, J. I. Cirac, and P. Zoller, Phys. Rev. A **62**, 023612 (2000).
- [57] A. Fetter, Annals of Physics **70**, 67 (1980).
- [58] J.-Q. Liao and C. K. Law, Phys. Rev. A **83**, 033820 (2011).
- [59] C. F. Van Loan, IEEE Transactions on Automatic Control **23**, 395 (1978).
- [60] M. Krämer, C. Menotti, L. Pitaevskii, and S. Stringari, Eur. Phys. J. D **27**, 247 (2003).
- [61] S. A. Gardiner, K. M. Gheri, and P. Zoller, Phys. Rev. A **63**, 051603(R) (2001).
- [62] V. B. Braginsky, *Measurement of Weak Forces in Physics Experiments* (Univ. of Chicago Press, Chicago, 1977); V. B. Braginsky, Y. I. Vorontsov, K. S. Thorne, Science **209**, 547 (1980).
- [63] F. Marquardt, A. A. Clerk and S. M. Girvin, J. Mod. Opt. **55**, 3329 (2008).
- [64] A. A. Clerk, M. H. Devoret, S. M. Girvin, F. Marquardt, and R. J. Schoelkopf, Rev. Mod. Phys. **82**, 1155 (2010).
- [65] A. A. Clerk, F. Marquardt, and J. G. E. Harris, Phys. Rev. Lett. **104**, 213603 (2010).
- [66] T. P. Purdy, D. W. C. Brooks, T. Botter, N. Brahms, Z.-Y. Ma, and D. M. Stamper-Kurn, Phys. Rev. Lett. **105**, 133602 (2010).
- [67] D. Nagy, P. Domokos, A. Vukics and H. Ritsch, Eur. Phys. J D **55**, 659 (2009).
- [68] D. F. Walls and G. J. Milburn, *Quantum Optics*, 2nd Edition, (Springer, Berlin, 2008).
- [69] B. M. Peden, Ph.D. Thesis, University of Colorado (2010).
- [70] A. Bohm, *Quantum Mechanics Foundations and Applications*, (Springer Verlag, Berlin, 2001).